Quantum mechanical modeling of magnon-phonon scattering heat transport across three-dimensional ferromagnetic/nonmagnetic interfaces

Hui Pan [●], Li-Ming Tang [●], and Ke-Qiu Chen [●][*]

Department of Applied Physics, School of Physics and Electronics, Hunan University, Changsha 410082, China

Magnon-phonon scattering (MPS) has attracted widespread attention in quantum heat/spin transport across the ferromagnetic/nonmagnetic (F/N) interfaces, with the rapid progress of experiments on spin caloritronics in recent years. However, the lack of theoretical methods, accounting for the MPS rigorously, has seriously hindered investigations on the quantum heat transport in magnetic nanostructures with broken translational symmetry, such as F/N interfaces. In this paper, we propose a theoretical formalism of the nonequilibrium Green function to incorporate the MPS into the quantum heat transport for three-dimensional ferromagnetic nanostructures, rigorously, through a diagrammatic perturbation analysis. A computational scheme is developed for the first-principles simulation of quantum heat transport in practical magnetic nanostructures, and a generalized formalism of heat flow is presented for the analysis of the elastic and inelastic process of heat transport. A thermal rectification driven by MPS is observed in the numerical simulation of heat transport across the F/N interface based on the CrI_3 monolayer, which is consistent with recent studies. In this paper, we open the gate to first-principles investigations of quantum heat transport in magnetic nanostructures and pave the way for the theoretical design of magnetic thermal nanodevices.

I. INTRODUCTION

The management and manipulation of heat transport in nanostructures has been a significant issue in nanoelectronics [1], thermoelectrics [2,3], and thermal devices [4,5]. In the past several decades, investigations of heat transport have mainly focused on the control of electrons and phonons [6–8] since they are the main carriers dominating transport of energy (electricity and heat) in most materials. With the rapid progress of spintronics [9,10] and spin caloritronics [11,12] in recent years, the spin degree of freedom has played an increasingly important role in the quantum heat transport of magnets [13–15]. One of the most attractive phenomena is the long-range spin transport in recent experiments of the spin Seebeck effect (SSE) [16,17] and acoustic spin pumping [18,19], which is attributed to the phonon drag effect [17] and has inspired studies of magnonpolarons [20–22], thermal Hall effect [23], and magnon-phonon scattering (MPS) [14,24]. Moreover, the modulation of phonon temperature through magnon-phonon interaction (MPI) has also been experimentally demonstrated in the spin Peltier effect, which provides insights for nanoscale cooling techniques [25]. The platforms of these studies are all around magnetic systems or ferromagnetic/nonmagnetic (F/N) interfaces, where MPS plays a critical role. Therefore, an in-depth understanding of MPS in magnetic nanostructures, especially in F/N interfaces [26], is momentous for both fundamental science and practical applications [27].

A full quantum mechanical simulation of MPS heat transport in practical magnetic nanostructures is still a huge challenge. Benefitting from the improvement of computing performance and the power of density functional theory (DFT) in the simulation of electronic structures and phonon properties of crystals [28], first-principles methods accounting for electron-phonon [29] and/or phonon-phonon scattering [30–32] have been developed, based on the semiclassical Boltzmann transport equation (BTE), for the transport simulation of crystals and bulk materials. The scattering-matrix method [33,34] and the nonequilibrium Green function (NEGF) method have also been introduced into the quantum transport simulation for nanoscale devices [35–39], whereas related research on MPS has gone at a slow pace. In recent years, fruitful efforts have been made through solving the BTE [40,41], as well as introducing spin degrees of freedom into classical [42] or *ab initio* [43] molecular dynamics (MD). In addition, methods based on first-principles [44,45] or random displacement from MD [46], which have been introduced into the electron-phonon scattering case [47], have also been developed for the evaluation of MPI strength as well as temperature dependence of magnon-phonon relaxation. However, these investigations have mainly focused on the relaxation time or energy modification of particles in bulk structures with a classical or semiclassical consideration, whereas the wave nature has been ignored, and these methods thus hardly serve for heat transport in nanoscale junctions [48] or typical F/N interfaces in SSE experiments [17]. Recently, several theoretical studies have concentrated on the coherent tuning of heat [49,50] or spin [51,52] transport across F/N junctions under an external magnetic field, through the introduction of the NEGF method into a one-dimensional (1D) model

*keqiuchen@hnu.edu.cn
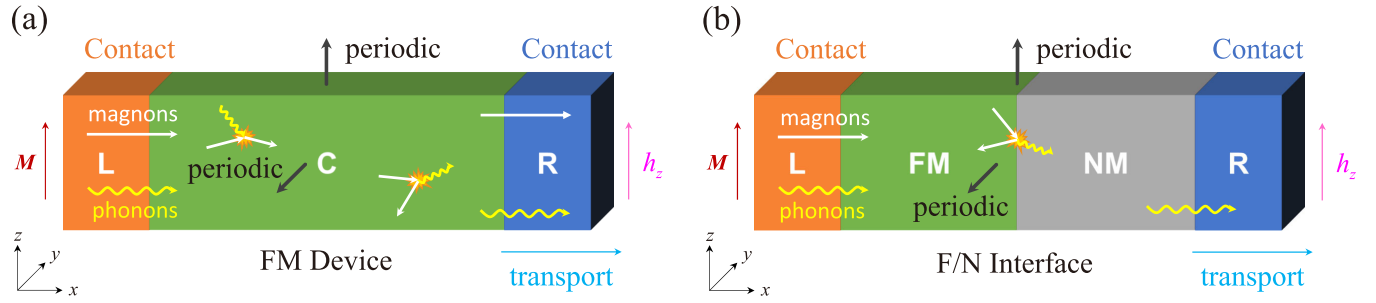
FIG. 1. Schematics of the physical model in the present three-dimensional (3D) nonequilibrium Green function (NEGF) formalism. (a) Ferromagnetic devices with a transverse periodicity. (b) Ferromagnetic/nonmagnetic (F/N) interfaces with a transverse periodicity; the magnetization (M) of the ferromagnetic region is assumed to point in the $+z$ direction. An external magnetic field along the $+z$ direction (h_z) is applied to all regions. The magnon-phonon scattering (MPS) is only considered in the central region (C). In the case of F/N interfaces, the energy of magnons can only be transferred from the left contact (Contact L) to the right contact (Contact R) via MPS.

system [53,54], and the thermal rectification [55–57] as well as negative differential thermal conductance (NDTC) [58,59] are observed. These studies have made some attempts at the quantum mechanical modeling of heat transport with MPS, whereas the first-principles investigation of the MPS heat transport in practical magnetic nanostructures is still challenging.

In this paper, based on the NEGF and the many-body perturbation theory, we propose a rigorous theoretical method as interfaced with first-principles calculations to accurately account for the MPS-related heat transport in the practical three-dimensional (3D) magnetic nanodevices, and we apply it to a two-dimensional (2D) F/N interface based on CrI$_3$ monolayer (ML) to investigate the phonon drag heat transport properties of magnons. Our numerical result agrees with the recent study [50] and thus provides valuable insights for the magnetic manipulation of heat transport. This paper is organized as follows: Firstly, we propose the theoretical formulations of Green's function and many-body self-energy, through a diagrammatic perturbation analysis in Sec. II, and a generalized formalism of heat flow is proposed for the separation of elastic and inelastic part contributions of heat flow in the multiparticle (and multiterminal) coupled system. To evaluate the degree of deviation from the equilibrium state in the central region of magnons, we propose a general formalism of the effective local temperature (ELT) for both phonons and magnons. In Sec. III, the effectiveness of the present methods are discussed and verified through applying the present NEGF formalism into a F/N interface based on the CrI$_3$ ML. Moreover, the computational details as interfaced with DFT are discussed for further verification and investigation. Finally, a summary is made in Sec. IV.

II. MODELS AND METHODOLOGY

In this section, we propose a NEGF formalism to incorporate the MPS into the quantum heat transport, in ferromagnetic nanodevices with a transverse periodicity. Firstly, in Sec. II A, we give the Hamiltonian of the magnon and phonon in reciprocal space. Then the theoretical formulations of Green's functions and self-energies for both spin and phonon systems are given in Sec. II B. Finally, in Sec. II C, the energy exchange in this magnon-phonon coupled system are discussed; meanwhile, a generalized formalism of heat flow and the ELT are suggested for further analysis.

A. Models and Hamiltonian

In this subsection, we build the quantum mechanical model for 3D nanodevices with the MPS in the central region and give the formalism of the Hamiltonian in reciprocal space. The simplified physical model for 3D ferromagnetic nanodevices with a transverse periodicity is shown in Fig. 1(a). We assume the magnetization (M) of the ferromagnetic region to point in the $+z$ direction in the ferromagnetic ground state. An external magnetic field along the $+z$ direction h_z is applied to the whole device. In the transport direction, the whole device connecting with two semi-infinite thermal contacts (L and R) is treated as a large unit cell, regardless of whether it satisfies translation symmetry. The MPS is assumed to only exist in the central region (C), where the noninteracting magnons and phonons from two semi-infinite contacts are scattered. Since the magnons and phonons are considered as the only thermal carriers in ferromagnetic insulators, the spin and vibration properties of such a device system can be described by the following Hamiltonian:

$$\hat{\mathcal{H}} = \hat{\mathcal{H}}_{sp} + \hat{\mathcal{H}}_{ph} + \hat{\mathcal{H}}_{sp-ph}, \quad (1)$$

where $\hat{\mathcal{H}}_{sp}$, $\hat{\mathcal{H}}_{ph}$ and $\hat{\mathcal{H}}_{sp-ph}$ are the Hamiltonian for spin, phonon, and spin-phonon coupling (SPC), respectively. For the spin system, the Heisenberg ferromagnetic model is adopted [cf. Eq. (A1) in Appendix A]. Applying the Holstein-Primakoff transformation [60] yields the magnon Hamiltonian in atomic representation as

$$\hat{\mathcal{H}}_{sp} = \sum_{m,n} \sum_{i,j} X_{i,j}(m,n) \hat{a}^{+}_{m,i} \hat{a}_{n,j}, \quad (2)$$

where $\hat{a}^{+}_i$ and $\hat{a}_i$ are the bosonic creation and annihilation operators of spin deviation (magnon), respectively, and $X_{i,j}(m,n)$ is the matrix element of the magnon Hamiltonian [cf. Eq. (A3) in Appendix A]. Here, m and n run over all the cells along the periodic direction, while i and j run over all the spin degrees of freedom in each cell. On the other hand, the phonon Hamiltonian is composed of the atomic kinetic energy

as well as the interatomic potential energy as

$$\hat{\mathcal{H}}_{ph} = \frac{1}{2}\sum_m \sum_i m_i \hat{\dot{u}}_{m,i} \hat{\dot{u}}_{m,i}$$
$$+ \frac{1}{2!}\sum_{m,n}\sum_{i,j} K_{i,j}(m,n)\hat{u}_{m,i}\hat{u}_{n,j}, \qquad (3)$$

where i and j, here, run over all the vibrational degrees of freedom in each cell. Also, m_i is the atomic mass, and $K_{i,j}(m,n)$ is the second-order force constant. Further, $\hat{u}_{m,i}$ and $\hat{\dot{u}}_{m,i}$ are the displacement and velocity operators, respectively.

As for the MPS term, we assume the MPI to only originate from the lowest perturbation of atomic vibration $u_{m,i}$ to the exchange coupling constant $J_{i,j}(m,n)$ [50,61,62], and thus, the MPS Hamiltonian in atomic representation reads

$$\hat{\mathcal{H}}_{sp-ph} = \sum_{m,n,l}\sum_{i,j,k} M_{i,j,k}(m,n,l)\hat{a}^+_{m,i}\hat{a}_{n,j}\hat{u}_{l,k}, \qquad (4)$$

where $M_{i,j,k}(m,n,l)$ is the first-order SPC constant [cf. Eq. (A12) in Appendix A]. Here, m, n, and l run over all the cells along the transverse direction in the central region since the MPS is only considered here. Also, i and j label the spin degrees of freedom in each cell, while k labels the atomic vibration degrees of freedom.

For a periodic system, it is more convenient to serve in reciprocal space to avoid processing a large amount of atoms in supercell, and we thus rewrite Eq. (1) in reciprocal space. The **k**-decomposed Hamiltonian of magnons reads

$$\hat{\mathcal{H}}_{sp} = \sum_{\mathbf{k}}\sum_{i,j} \mathcal{X}_{i,j}(\mathbf{k})\hat{a}^\dagger_{\mathbf{k},i}\hat{a}_{\mathbf{k},j}, \qquad (5)$$

and the **q**-decomposed Hamiltonian of phonons is found to be

$$\hat{\mathcal{H}}_{ph} = \sum_{\mathbf{q}}\sum_{i,j} \mathcal{K}_{i,j}(\mathbf{q})\hat{u}_{-\mathbf{q},i}\hat{u}_{\mathbf{q},j}, \qquad (6)$$

where $\mathbf{k} = (0, k_y, k_z)$ and $\mathbf{q} = (0, q_y, q_z)$ are the transverse wave vectors of magnons and phonons in the yz plane, respectively. Here, $\mathcal{X}_{i,j}(\mathbf{k})$ and $\mathcal{K}_{i,j}(\mathbf{q})$ denote the matrix elements of $\hat{\mathcal{H}}_{sp}$ and $\hat{\mathcal{H}}_{ph}$ in reciprocal space [cf. Eqs. (A6) and (A10) in Appendix A]. Also, $\hat{a}^\dagger_{\mathbf{k},i}$ and $\hat{a}_{\mathbf{k},i}$ are the **k**-components of $\hat{a}^+_{m,i}$ and $\hat{a}_{m,i}$, respectively, while $\hat{u}_{\mathbf{q},i}$ is the **q**-component of the displacement operator $\hat{u}_{m,i}$. The transformation details can be found in Appendix A. Following the above transformation, the SPC term of the Hamiltonian [cf. Eq. (A11) in Appendix A] can also be rewritten in reciprocal space as

$$\hat{\mathcal{H}}_{sp-ph} = \sum_{\mathbf{k},\mathbf{q}}\sum_{i,j,k} \mathcal{M}_{i,j,k}(\mathbf{k},\mathbf{q})\hat{a}^\dagger_{\mathbf{k},i}\hat{a}_{\mathbf{k}-\mathbf{q},j}\hat{u}_{\mathbf{q},k}, \qquad (7)$$

where $\mathcal{M}(\mathbf{k},\mathbf{q})$ is the coupling matrix in reciprocal space [cf. Eq. (A15) in Appendix A]. The conservation of momentum is naturally satisfied since the summation of the wave vectors of all annihilation operators in Eq. (7) is always equal to that of the creation operators: $\mathbf{k} = (\mathbf{k} - \mathbf{q}) + \mathbf{q}$. In addition, the above expressions of the Hamiltonian in reciprocal space also work for 2D devices with a transverse periodicity along the y direction, while the only change is to let $k_z = 0$ and $q_z = 0$.

The only input parameters for the present NEGF formalism are $\mathcal{X}$, $\mathcal{K}$, and $\mathcal{M}$. In this paper, they are obtained from the

numerical calculations based on first-principles calculations, which will be discussed in Sec. III C. To facilitate the calculation of Green's functions, we rewrite each **k**-component of the magnon Hamiltonian matrix as the block representation:

$$\mathcal{X}(\mathbf{k}) = \begin{pmatrix} \mathcal{X}_L & \mathcal{U}_{LC} & 0 \\ \mathcal{U}_{CL} & \mathcal{X}_C & \mathcal{U}_{CR} \\ 0 & \mathcal{U}_{RC} & \mathcal{X}_R \end{pmatrix}(\mathbf{k}), \qquad (8)$$

and the one for the phonon reads

$$\mathcal{K}(\mathbf{q}) = \begin{pmatrix} \mathcal{K}_L & \mathcal{V}_{LC} & 0 \\ \mathcal{V}_{CL} & \mathcal{K}_C & \mathcal{V}_{CR} \\ 0 & \mathcal{V}_{RC} & \mathcal{K}_R \end{pmatrix}(\mathbf{q}), \qquad (9)$$

where $\mathcal{X}_L$ ($\mathcal{K}_L$), $\mathcal{X}_C$ ($\mathcal{K}_C$), and $\mathcal{X}_R$ ($\mathcal{K}_R$) denote the magnon (phonon) Hamiltonian matrices of the left contact (L), central region (C), and right contact (R), respectively. Here, $\mathcal{U}$ ($\mathcal{V}$) denotes the coupling matrix between the contact and the central region of the magnon (phonon) system. It is notable that, for a 3D F/N interface as shown in Fig. 1(b), there is no magnon in the nonmagnetic region (contact R). In this case, the block representation of the magnon Hamiltonian matrix reads

$$\mathcal{X}(\mathbf{k}) = \begin{pmatrix} \mathcal{X}_L & \mathcal{U}_{LC} \\ \mathcal{U}_{CL} & \mathcal{X}_C \end{pmatrix}(\mathbf{k}), \qquad (10)$$

and the heat energy of magnons in the ferromagnetic region (L and C) can only be transferred to the phonons in the nonmagnetic region (contact R) through MPS.

B. Green's functions and self-energies for MPS

In this subsection, we define the contour-ordered Green's functions of the magnon and phonon as well as yield the theoretical formulation of self-energy for MPS through a diagrammatic perturbation expansion for 3D devices, as shown in Fig. 1. For a periodic system, we define the contour-ordered Green function of the magnon and phonon as

$$G_{i,j}(\mathbf{k};\tau,\tau') = -\frac{i}{\hbar}\langle T_C[\hat{a}_{H;\mathbf{k},i}(\tau)\hat{a}^\dagger_{H;\mathbf{k},j}(\tau')]\rangle, \qquad (11)$$

$$D_{i,j}(\mathbf{q};\tau,\tau') = -\frac{i}{\hbar}\langle T_C[\hat{u}_{H;\mathbf{q},i}(\tau)\hat{u}_{H;-\mathbf{q},j}(\tau')]\rangle, \qquad (12)$$

where **k** and **q** are the transverse wave vectors of magnons and phonons, respectively. Here, τ and τ' are time on contour, while T_C is the contour-ordering operator. The contour-ordered Green function is defined in the Heisenberg picture, and $\langle \cdots \rangle$ denotes the grand canonical ensemble average [63].

For an unperturbed case, we assume the central region to be in the equilibrium state where neither heat contacts nor MPS are incorporated. In this way, the unperturbed retarded Green function of the magnon in matrix notation is found to be [cf. Eqs. (B21) and (B17) in Appendix B 1]

$$\mathbf{G}^{(0),R}(\mathbf{k},\varepsilon) = [(\varepsilon + i\eta)\mathbf{I} - \mathcal{X}_C(\mathbf{k})]^{-1}, \qquad (13)$$

and the one for the phonon reads

$$\mathbf{D}^{(0),R}(\mathbf{q},\omega) = [(\omega + i\eta)^2\mathbf{I} - \mathcal{K}_C(\mathbf{q})]^{-1}, \qquad (14)$$

where ε and $\hbar\omega$ are the energies for the magnon and phonon, respectively, and η denotes a positive infinitesimal. Here, **I**

and -1 denote the identity matrix and the matrix inversion, respectively. The derivation details of the presented unperturbed Green function can be found in Appendix B 1.

Once the perturbation from heat contacts or MPS is considered, the perturbed Green's functions of the magnon are given by Dyson's equation based on the Keldysh formalism [64] as

$$\mathbf{G}^R(\mathbf{k}, \varepsilon) = [\mathbf{G}^{(0),R}(\mathbf{k}, \varepsilon)^{-1} - \mathbf{\Sigma}^R(\mathbf{k}, \varepsilon)]^{-1}, \quad (15)$$

$$\mathbf{G}^{>,<}(\mathbf{k}, \varepsilon) = \mathbf{G}^R(\mathbf{k}, \varepsilon)\mathbf{\Sigma}^{>,<}(\mathbf{k}, \varepsilon)\mathbf{G}^A(\mathbf{k}, \varepsilon), \quad (16)$$

where $\mathbf{\Sigma} = \mathbf{\Sigma}_T + \mathbf{\Sigma}_M$ is the total self-energy. Here, $\mathbf{\Sigma}_T = \mathbf{\Sigma}_L + \mathbf{\Sigma}_R$ is the self-energy from the semi-infinite thermal contacts of magnons, while $\mathbf{\Sigma}_M$ originates from MPS. The surface self-energy of contact α (L or R) can be obtained from $\mathbf{\Sigma}_\alpha = \mathcal{U}_{C\alpha} g_\alpha \mathcal{U}_{\alpha C}$, where the surface Green function g_α can be computed rigorously via recursive iterations [65,66] or the decimation technique [67]. By the way, for a F/N interface as shown in Fig. 1(b), there is only one effective thermal contact (Contact L) for the magnon system because of the nonmagnetism of the right contact (Contact R), and thus, $\mathbf{\Sigma}_T = \mathbf{\Sigma}_L$. For the phonon system, we also have

$$\mathbf{D}^R(\mathbf{q}, \omega) = [\mathbf{D}^{(0),R}(\mathbf{q}, \omega)^{-1} - \mathbf{\Pi}^R(\mathbf{q}, \omega)]^{-1}, \quad (17)$$

$$\mathbf{D}^{>,<}(\mathbf{q}, \omega) = \mathbf{D}^R(\mathbf{q}, \omega)\mathbf{\Pi}^{>,<}(\mathbf{q}, \omega)\mathbf{D}^A(\mathbf{q}, \omega), \quad (18)$$

and $\mathbf{\Pi} = \mathbf{\Pi}_T + \mathbf{\Pi}_M$ is the total self-energy of phonons. The self-energy from contacts α can also be obtained from $\mathbf{\Pi}_\alpha = \mathcal{V}_{C\alpha} d_\alpha \mathcal{V}_{\alpha C}$, where d_α is the phonon surface Green function of contact α. For ballistic transport problems, only the retarded Green function and self-energy from contacts are necessary to obtain the transmission through the system via the Caroli formula [66,68] since the many-body terms of the self-energy ($\mathbf{\Sigma}_M$ and $\mathbf{\Pi}_M$) vanish.

The crucial point of solving transport problems with MPS is to determine the scattering terms of self-energy $\mathbf{\Sigma}_M$ and $\mathbf{\Pi}_M$. Although the expressions of MPS self-energies for the 1D system have been proposed in a recent study [50], a rigorous expression for the 3D case in the literature is lacking, which is also the primary motivation for this paper. In this paper, through a diagrammatic perturbation expansion [cf. Eqs. (B25)–(B29) in Appendix B 2], we obtain the rigorous formulation of the greater/lesser scattering self-energy for magnons as

$$\Sigma_{i,m}^{>,<}(\mathbf{k}, \varepsilon) = i\hbar \sum_{\mathbf{q}} \mathcal{M}_{i,j,k}(\mathbf{k}, \mathbf{q})\mathcal{M}_{l,m,n}(\mathbf{k} - \mathbf{q}, -\mathbf{q})$$
$$\times \int_{-\infty}^{+\infty} \frac{d\omega}{2\pi} G_{j,l}^{>,<}(\mathbf{k} - \mathbf{q}, \varepsilon - \hbar\omega)D_{k,n}^{>,<}(\mathbf{q}, \omega), \quad (19)$$

and the retarded term reads

$$\Sigma_{i,m}^{R}(\mathbf{k}, \varepsilon) = i\hbar \sum_{\mathbf{q}} \mathcal{M}_{i,m,k}(\mathbf{k}, \mathbf{q})\mathcal{M}_{l,m,n}(\mathbf{k} - \mathbf{q}, -\mathbf{q})$$
$$\times \int_{-\infty}^{+\infty} \frac{d\omega}{2\pi} \big[G_{j,l}^{R}(\mathbf{k} - \mathbf{q}, \varepsilon - \hbar\omega)D_{k,n}^{>}(\mathbf{q}, \omega)$$
$$+ G_{j,l}^{<}(\mathbf{k} - \mathbf{q}, \varepsilon - \hbar\omega)D_{k,n}^{R}(\mathbf{q}, \omega) \big]. \quad (20)$$
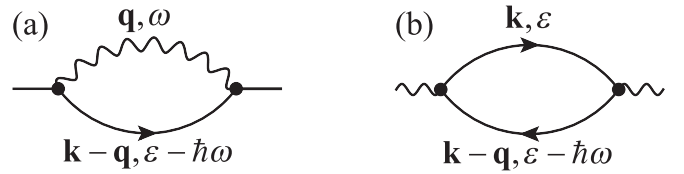
FIG. 2. Feynman diagrams for the magnon-phonon scattering self-energies in energy-momentum space of (a) magnons and (b) phonons under the self-consistent Born approximation (SCBA). The straight and wavy lines represent the full Green's functions of magnons and phonons, respectively.

A clear derivation process for the presented MPS self-energies is detailed in Appendix B 2. The relevant diagrammatic representation for scattering self-energy of magnons in energy-momentum space is shown in Fig. 2(a). Unlike with the recent study in 1D spin-phonon junction [50], we ignore the Hartree term here since it donates a static potential from the lattice [69] and usually contributes nothing to transport in the periodic system [70]. Figure. 2(b) shows the diagrammatic representation of the scattering self-energy for phonons, and the greater/lesser self-energy is written as

$$\Pi_{k,n}^{>,<}(\mathbf{q}, \omega) = i \sum_{\mathbf{k}} \mathcal{M}_{i,j,k}(\mathbf{k} - \mathbf{q}, -\mathbf{q})\mathcal{M}_{l,m,n}(\mathbf{k}, \mathbf{q})$$
$$\times \int_{-\infty}^{+\infty} \frac{d\varepsilon}{2\pi} G_{j,l}^{>,<}(\mathbf{k}, \varepsilon)G_{m,i}^{<,>}(\mathbf{k} - \mathbf{q}, \varepsilon - \hbar\omega), \quad (21)$$

and the retarted term reads

$$\Pi_{k,n}^{R}(\mathbf{q}, \omega) = i \sum_{\mathbf{k}} \mathcal{M}_{i,j,k}(\mathbf{k} - \mathbf{q}, -\mathbf{q})\mathcal{M}_{l,m,n}(\mathbf{k}, \mathbf{q})$$
$$\times \int_{-\infty}^{+\infty} \frac{d\varepsilon}{2\pi} \big[G_{j,l}^{R}(\mathbf{k}, \varepsilon)G_{m,i}^{<}(\mathbf{k} - \mathbf{q}, \varepsilon - \hbar\omega)$$
$$+ G_{j,l}^{<}(\mathbf{k}, \varepsilon)G_{m,i}^{A}(\mathbf{k} - \mathbf{q}, \varepsilon - \hbar\omega) \big]. \quad (22)$$

Note that the diagrams suggested here are like that in the previous study of electron-phonon scattering [71] except with a sign difference since the electron is fermionic while the magnon is bosonic. It is inappropriate to apply a lowest-order expansion adopted in the electron-phonon case [72] since the energy scales of magnons and phonons are close, and the scattering self-energies of both sides are not negligible. Since the self-consistent Born approximation (SCBA) [53,73] is adopted in the derivation of the scattering self-energies, Eqs. (15)–(22) constitute a set of self-consistent equations, which has to be solved iteratively. The present NEGF formalism for 3D nanostructures can also be obtained through applying the lattice Fourier transform, which has been adopted in recent works about the 3D anharmonic phonon NEGF formalism [38,39], to the 1D NEGF formalism [50]. Nevertheless, the present derivation starting from the definition of the contour-ordered Green function in reciprocal space provides a more concise and physical perspective, while it can be further introduced into the building of 3D NEGF formalism for other kinds of scattering without the dependence on the formalism of the 1D case. Moreover, both the energy and

momentum conservation are naturally satisfied in the expressions of the scattering self-energies.

C. Energy exchange and ELT

In this subsection, we first discuss the energy exchange in the magnon-phonon coupled system. Once the greater and lesser Green's functions, as introduced in Sec. II B, are determined, the heat flow density of the magnon system flowing out of contact α is then given by the Meir-Wingreen formula [68,74] as

$$J_\alpha^m(\mathbf{k}, \varepsilon) = -\frac{\varepsilon}{2\pi} \text{Tr}[\mathbf{G}^>(\mathbf{k}, \varepsilon)\boldsymbol{\Sigma}_\alpha^<(\mathbf{k}, \varepsilon) - \mathbf{G}^<(\mathbf{k}, \varepsilon)\boldsymbol{\Sigma}_\alpha^>(\mathbf{k}, \varepsilon)], \quad (23)$$

where Tr denotes the matrix trace and the one for the phonon reads

$$J_\alpha^p(\mathbf{q}, \omega) = -\frac{\hbar\omega}{2\pi} \text{Tr}[\mathbf{D}^>(\mathbf{q}, \omega)\boldsymbol{\Pi}_\alpha^<(\mathbf{q}, \omega) - \mathbf{D}^<(\mathbf{q}, \omega)\boldsymbol{\Pi}_\alpha^>(\mathbf{q}, \omega)], \quad (24)$$

and the integral of the heat flow density to the energy yields the heat flow:

$$I_\alpha^m = \frac{1}{N} \sum_{\mathbf{k}} \int_0^{+\infty} \frac{d\varepsilon}{\hbar} J_\alpha^m(\mathbf{k}, \varepsilon), \quad (25)$$

$$I_\alpha^p = \frac{1}{N} \sum_{\mathbf{q}} \int_0^{+\infty} d\omega J_\alpha^p(\mathbf{q}, \omega), \quad (26)$$

where N is the number of k points.

The heat flow from one physical contact (Contact L or R) in the magnon (or phonon) system can be separated into two parts: one part is flowing to the other contacts directly, which is called the *elastic process*, while another is injected into (or released from) the phonon (or magnon) system via the MPS, which is called the *inelastic process* in the field of electron-phonon coupled transport [70]. To clarify the energy exchange relation in the present magnon-phonon coupled system, we present a generalized formalism of energy flow density:

$$\mathcal{J}_{\alpha\to\beta}^x(\mathbf{k}, \mathcal{E}) = -\frac{\mathcal{E}}{2\pi} \text{Tr}[\mathcal{G}_\beta^>(\mathbf{k}, \mathcal{E})\mathcal{S}_\alpha^<(\mathbf{k}, \mathcal{E}) - \mathcal{G}_\beta^<(\mathbf{k}, \mathcal{E})\mathcal{S}_\alpha^>(\mathbf{k}, \mathcal{E})], \quad (27)$$

and the corresponding heat flow reads

$$\mathcal{I}_{\alpha\to\beta}^x = \frac{1}{N\hbar} \sum_{\mathbf{k}} \int_0^\infty \mathcal{J}_{\alpha\to\beta}^x(\mathbf{k}, \mathcal{E}) d\mathcal{E}, \quad (28)$$

where $\mathcal{E}$, $\mathcal{G}$, and $\mathcal{S}$ are the energy, Green's function, and self-energy for each system, respectively, while x labels the magnon (m) or phonon (p) system. Here, α and β label the self-energy as contributed by thermal contact (L or R) or MPS (M). The generalized greater/lesser Green function $\mathcal{G}_\beta^{>,<}(\mathbf{k}, \mathcal{E})$ is defined as

$$\mathcal{G}_\beta^{>,<}(\mathbf{k}, \mathcal{E}) = \mathcal{G}^R(\mathbf{k}, \mathcal{E})\mathcal{S}_\beta^{>,<}(\mathbf{k}, \mathcal{E})\mathcal{G}^A(\mathbf{k}, \mathcal{E}). \quad (29)$$

In this way, the self-energy for MPS looks like a virtual contact which connects the magnon and phonon system. Figure 3
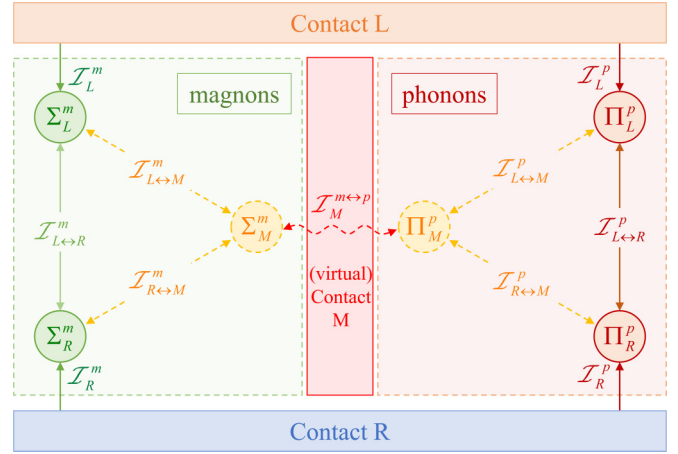
FIG. 3. Schematic of the energy exchange in the present magnon-phonon scattering (MPS) devices. The solid and dashed lines represent elastic and inelastic heat flow, respectively. The wavy line represents the energy exchange between magnons and phonons through MPS. The MPS acts as a virtual contact (Contact M) to exchange the heat energy between magnons and phonons.

shows the energy exchange net in the present magnon-phonon coupled system.

In addition, according to Eq. (27), the heat flow density satisfies the following antisymmetric relation:

$$\mathcal{J}_{\alpha\to\beta}^x(\mathbf{k}, \mathcal{E}) = -\mathcal{J}_{\beta\to\alpha}^x(\mathbf{k}, \mathcal{E}), \quad (30)$$

where the antisymmetry implies the directionality of energy flow. We can also further obtain $\mathcal{J}_{\alpha\to\alpha}^x = 0$ since there is no contact supplying energy flow to itself. The total energy flow density from contact α is given by

$$\mathcal{J}_\alpha^x(\mathbf{k}, \mathcal{E}) = \sum_\beta \mathcal{J}_{\alpha\to\beta}^x(\mathbf{k}, \mathcal{E}), \quad (31)$$

which precisely gives the same results with Eqs. (23) and (24) for the physical contacts (L and R). The energy exchange between magnons and phonons is given by the heat flow densities from virtual contacts $\mathcal{J}_M^m$ and $\mathcal{J}_M^p$. It should be noted that heat flows injected from virtual contact (M) into two systems are equal and opposite $I_M^m = -I_M^p$, while the heat flow densities are not $\mathcal{J}_M^m \neq -\mathcal{J}_M^p$. According to Eq. (30), we can further obtain the heat flow conservation relation:

$$\sum_\alpha \mathcal{I}_\alpha^x = \sum_\alpha \mathcal{J}_\alpha^x(\mathbf{k}, \mathcal{E}) = 0. \quad (32)$$

For a F/N interface device as shown in Fig. 1(b), there is only one effective physical contact (Contact L) in the magnon system, and we thus have $\mathcal{J}_L^m = \mathcal{J}_{L\to M}^m$ according to Eq. (31). This indicates that the heat energy of magnons from the ferromagnetic region can only be transferred to the nonmagnetic region via MPS. Moreover, to evaluate the degree of deviation from the equilibrium state in the central region of magnons, we introduce the ELT [75,76] and propose a general formalism of the ELT for both phonons and magnons. For heat transport problems, the ELT can be determined via the

equation of local energy conservation:

$$\int_0^\infty \mathcal{P}(\mathcal{E})\mathcal{E}d\mathcal{E} = \int_0^\infty f_B(\mathcal{E}, T_e)\mathcal{D}(\mathcal{E})\mathcal{E}d\mathcal{E}, \qquad (33)$$

where $\mathcal{P}$ and $\mathcal{D}$ are the local density of population (LDOP) and local density of states (LDOS), respectively. Here, f_B is the Bose-Einstein distribution, and T_e is the ELT to be determined. The LDOS is given by

$$\mathcal{D}(\mathcal{E}) = -\frac{\mathcal{E}^{n-1}}{\pi}\frac{1}{N}\sum_{\mathbf{k}}\text{Tr}\{\text{Im}[\mathcal{G}^R(\mathbf{k}, \mathcal{E})]\}, \qquad (34)$$

while the LDOP reads

$$\mathcal{P}(\mathcal{E}) = -\frac{\mathcal{E}^{n-1}}{2\pi}\frac{1}{N}\sum_{\mathbf{k}}\text{Tr}\{\text{Im}[\mathcal{G}^<(\mathbf{k}, \mathcal{E})]\}, \qquad (35)$$

where $n = 1, 2$ are for magnons and phonons, respectively, and Im means the imaginary part. The ELT T_e is the solution of Eq. (33). Once the ELT of the magnon in the central region T_C^m is determined, the temperature deviation of magnons between the left contact and the central region is defined as

$$\Delta T_{\text{drag}}^m = T_L^m - T_C^m, \qquad (36)$$

which is shown to be a significant index to evaluate the strength of the phonon drag effect in the numerical analysis of Sec. III.

III. RESULTS AND DISCUSSIONS

In this section, we will focus on the inelastic heat transport behaviors of magnons and phonons across the F/N interface, under the tuning of external conditions (temperature and magnetic field), and some perspectives and applications of the present NEGF formalism will be discussed. Firstly, in Sec. III A, the relation between the spin frozen phenomenon and the thermal rectification is discussed, and the temperature deviation of magnons is proposed to evaluate the strength of the phonon drag effect. To further reveal the microscopic mechanism of phonon drag magnon heat transport, Sec. III B shows the magnetic-field-dependent LDOS and heat flow density, and the energy transfer on a spectrum level is discussed. Finally, in Sec. III C, the input setting and numerical details based on first-principles calculations are shown for further verification, and some perspectives of the present NEGF formalism are discussed for further studies.

A. Spin frozen phenomenon, thermal rectification, and NDTC

In this subsection, we apply the present method to a F/N interface based on CrI$_3$ ML, which has been reported as a 2D magnetic material with strong spin-lattice coupling in recent studies [77]. The schematic of the numerical model for this device is shown in Fig. 4(a), where the device is periodic along the y axis, and the entire device is placed under an external magnetic field along the $+z$ direction (h_z). To simulate the heat transport property of a practical F/N interface corresponding to the physical model as shown in Fig. 1(b), we assume the right contact region (Contact R) is nonmagnetic but keep the same site configuration with CrI$_3$, which saves computational cost by avoiding the DFT step of the practical F/N interface, and this has almost no impact on the presentation of this
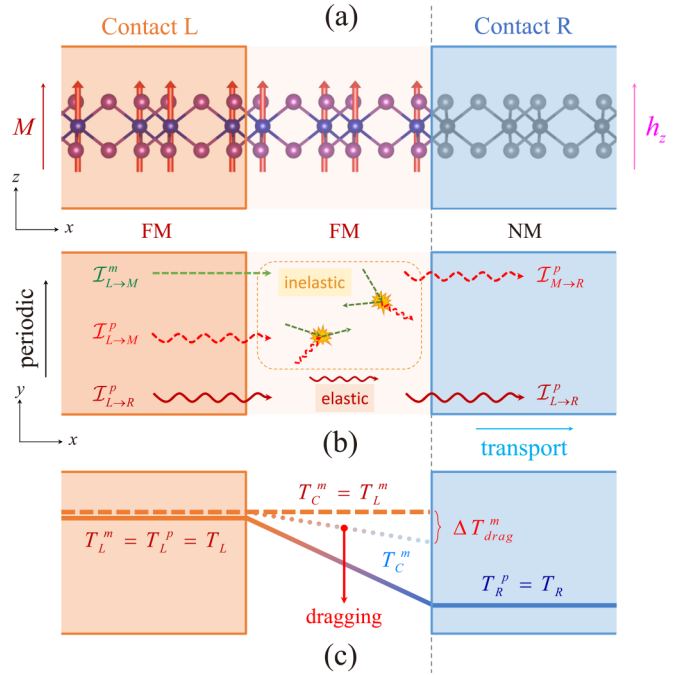
FIG. 4. Heat transport through the present ferromagnetic/nonmagnetic (F/N) interface based on CrI$_3$ monolayer (ML). (a) Schematic of the numerical model; the transverse direction (y direction) of this device is periodic, and an external magnetic field pointing in the $+z$ direction is applied to the whole device; the nonmagnetic region (Contact R) is assumed to have the same site configuration as CrI$_3$ but to be nonmagnetic. (b) Schematic of the heat flow across the present F/N interface device; the dashed (or solid) straight line with arrow and the dashed (or solid) wavy line with arrow denote the inelastic (or elastic) heat flow of magnons and phonons, respectively. (c) Schematic of the temperature deviation of the magnons as induced by the nonequilibrium phonons; the dashed and dotted lines denote the effective local temperature (ELT) of magnons without and with magnon-phonon scattering, respectively, and the solid line denotes the ELT of phonons.

paper. In such a F/N interfacial device, no energy can be exchanged via magnons between the left contact (Contact L) and the right contact (Contact R) without the assistance of a phonon. Similar cases of electron-phonon scattering have been studied in a 1D model system [78]. The heat transport of magnons across such a F/N interface originates from the nonequilibrium potential as dragged by phonons, and such an interfacial heat transport behavior of magnons is important to understand some experiments in spin caloritronics [16–19]. Figure 4(b) shows the schematic of heat flow across this magnon-phonon coupled F/N interface. According to the conservation relations as introduced in Sec. II C, the total inelastic heat flow injected from the left contact is always equal to that flowing out of the right contact $\mathcal{I}_{L\to M}^m + \mathcal{I}_{L\to M}^p = \mathcal{I}_{M\to R}^p$, which indicates that some heat energies are transferred from magnons to phonons via the MPS process. To evaluate the degree to which magnons deviate from the equilibrium state as induced by nonequilibrium phonons, we also employ the temperature deviation of magnons as introduced in Sec. II C. The schematic of the ELT distribution is shown in Fig. 4(c). In
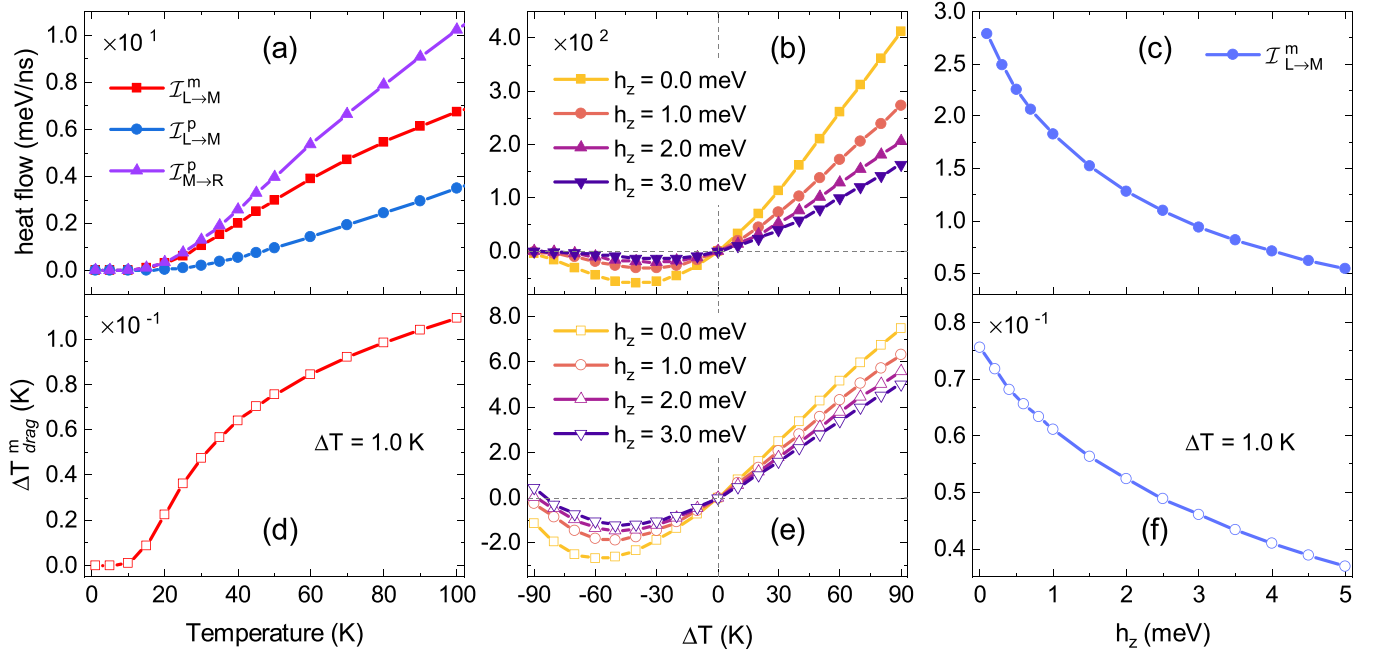
FIG. 5. The temperature, temperature difference, and external magnetic field dependence of (a)–(c) inelastic heat flow and (d)–(f) phonon drag temperature deviation of magnons. A temperature difference of 1 K is used in (a), (c), (d), and (f). A magnetic field of 0.0 meV is adopted in (a) and (d). A central temperature of 50 K is used in (b), (c), (e), and (f).

the ballistic case (dashed line), the magnon system is actually in an equilibrium state, and the ELT of magnons in the central region (T_C^m) is the same as that in the left contact (T_L^m). Once MPS is considered (dotted line), the magnons in the central region will transfer energy to phonons and will be dragged into a nonequilibrium state. Meanwhile, a temperature deviation ($\Delta T_{\mathrm{drag}}^m$) between the central region and the left contact will arise in the magnon system. By the way, in this paper, we mainly focus on the phonon-mediated magnon heat transport (inelastic heat transport) across the F/N interfaces since it intuitively shows the nonlinear energy exchange behaviors of magnons and phonons at the F/N interfaces.

First, we show the spin frozen phenomenon in the magnon-related heat transport. The temperature dependence of inelastic heat flow is shown in Fig. 5(a). It is obvious that the inelastic heat flow of both magnons and phonons is ∼0 under 10 K, which is consistent with the recent theoretical study [50] of heat transport across a 1D spin-phonon junction model and is attributed to the exponential dispersion and weak scattering of magnons in low temperature. To further demonstrate this point of view, we show the temperature deviation of magnons ($\Delta T_{\mathrm{drag}}^m$) in Fig. 5(d). Here, $\Delta T_{\mathrm{drag}}^m$ is close to zero in the low-temperature region (<10 K). This result means that the state of magnons between the central region and the left contact is close, with an equilibrium distribution of magnons, and this indicates a weak MPS in the central region at low temperature. In addition, as the temperature rises, $\Delta T_{\mathrm{drag}}^m$ shows a similar dependence with the heat flow of magnons, which demonstrates the effectiveness of temperature deviation on the evaluation of the phonon drag effect. To clarify the relation between spin frozen and nonreciprocal heat transport, we further show the dependence of magnon heat flow on temperature difference under different external magnetic fields in Fig. 5(b). Due to the asymmetric setting of

the magnon system, the thermal rectification effect and NDTC arise. To be more specific, the appearance of NDTC is the result of competition between the temperature difference of the device and the temperature of the left contact: T_L^m reduces as ΔT decreases. Different from the ballistic case, inelastic heat flows reduce sharply as the temperature decreases, which results in the reduction of $\mathcal{I}_{L \to M}^m$ after $\Delta T < -50$ K. Furthermore, the turning point of $\mathcal{I}_{L \to M}^m$ shifts to zero as h_z increases, which also confirms that the spin frozen phenomenon strengthens the thermal rectification and NDTC. Incidentally, the decrease of central temperature [50] exhibits a similar effect as the increase of h_z since both means aim to let T_L in the spin frozen temperature region under a smaller ΔT. The temperature deviation of magnons, as shown in Fig. 5(e), is also consistent with Fig. 5(b).

Moreover, the spin frozen phenomenon via the external magnetic field has been adopted in heat conductance experiments of magnetic materials to distinguish the contributions of magnons and phonons [14]. Figures 5(c) and 5(f) show the h_z dependence of heat flow and temperature deviation of magnons, respectively. It is notable that the inelastic heat flow reduces about six times as h_z increases from 0.0 to 5.0 meV, which demonstrates the application potential in magnetic thermal switching [79]. The present $\Delta T_{\mathrm{drag}}^m$ is expected to be experimentally demonstrated in magnon thermometry experiments [80].

B. LDOS and heat flow density manipulated by an external magnetic field

To further reveal the microscopic mechanism of phonon drag magnon heat transport and explain the results discussed in Sec. III A, in this subsection, we discuss the features of the LDOS and heat flow density under an external magnetic field.
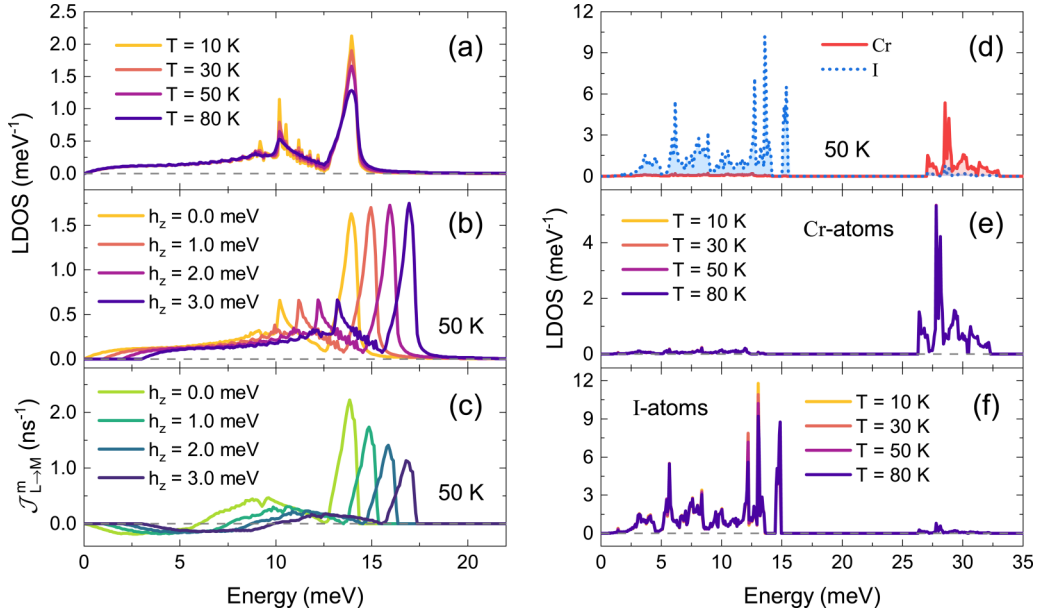
FIG. 6. The local density of states (LDOS) of magnons (a) at different central temperatures with $h_z = 0$ meV; (b) under different magnetic field h_z at 50 K. (c) shows the h_z-dependent heat flow density of magnons at 50 K. (d)–(f) show the LDOS of phonons donated by (e) Cr and (f) I atoms, respectively, at different temperature with $h_z = 0$ meV.

It should be noted that the inelastic heat flow of phonons is far smaller than the elastic one [see Fig. 10(b) in Appendix C]. To explain this, we show the LDOS of magnons and phonons in Figs. 6(a) and 6(d), respectively. Firstly, it is seen that the maximum energy of phonons is ~32 meV, which is consistent with recent studies [46,81] and is approximately twice that of magnons [see also Fig. 10(a) in Appendix C]. However, due to the conservation of energy in the process of MPS as shown in Fig. 2 of Sec. II B, phonons with energy >15 meV cannot be absorbed or emitted by any magnon, which implies that the impact of MPS to magnons is stronger than that to phonons. Moreover, the low-frequency vibration is mainly contributed by the I atoms, while the magnetic atoms (Cr) mainly donate to high-frequency vibration. The above two factors determine that the MPS in CrI_3 ML is weak and impacts magnons stronger than phonons. In addition, the temperature-dependent LDOS of magnons and phonons as shown in Figs. 6(a), 6(e), and 6(f) demonstrate it. As the central temperature rises, the magnons with high energy ($\varepsilon > 10$ meV) are scattered strongly since the LDOS decreases obviously. Meanwhile, for phonons, the LDOS in the low-energy region ($\hbar\omega < 15$ meV) only decreases a little, while the LDOS of the high-energy phonon hardly changes.

To further reveal the nature of the h_z dependence of thermal rectification and NDTC as shown in Fig. 5, the LDOS and heat flow density of magnons under different external magnetic fields are shown in Figs. 6(b) and 6(c), respectively. The whole energy of the magnons increases with the increase of h_z, which results in less excitation of magnons at the same temperature. As a matter of fact, the energy shift originates from the on-site contribution of h_z to X [cf. Eq. (A3) in Appendix A], while the increase of the LDOS in the high-energy region indicates an attenuation of scattering strength. These results also demonstrate that the increase of h_z plays a similar role with the decrease of central temperature, in both the thermal

rectification and the NDTC. As a result, the magnitude of heat flow density as shown in Fig. 6(c) decreases with the increase of external magnetic field. Moreover, it is attractive that the magnons with low energy ($\varepsilon < 6$ meV when $h_z = 0.0$ meV) donate a negative heat flow density, while the magnons in the high-energy region ($\varepsilon > 6$ meV when $h_z = 0.0$ meV) contribute a positive one. This result indicates the conservation magnon number, and there is no magnon passing through the present F/N interface. Consequently, the microprocess of the phonon drag heat transport in a F/N interface is as follows: As the temperature rises, magnons and phonons interact without an observable energy exchange, as well as both magnons and phonons are in an equilibrium state when $\Delta T = 0$. When $\Delta T \neq 0$, the magnons and phonons in each contact are still in equilibrium state, while magnons and phonons in the central region are not due to the energy exchange between magnons and phonons via MPS. The higher temperature of magnons determines that magnons in the central region only have to transfer energy to phonons. Owing to the conservation of magnon number in the present MPS process, the magnon with higher energy emits a phonon and turns into another lower-energy magnon. The schematic for the microprocess of energy transfer from magnons to phonons is shown in Fig. 7. In this way, the MPS vertex plays the role of a converter, which absorbs the energy of magnons from the left contact and releases more phonons to the right contact. The thick lines in the diagrammatic representation of MPS mean the accumulation of both low-energy magnons and phonons in the central region of the device. Moreover, the present results show that MPS actually contributes little to the total heat transport, even though the SPC is reported to be strong in CrI_3 ML. There are two principal reasons for this difference. On the one hand, static modification of SPC to the dispersion of phonons has been considered in the step of finite displacements based on the spin-polarized DFT calculations. A detailed discussion
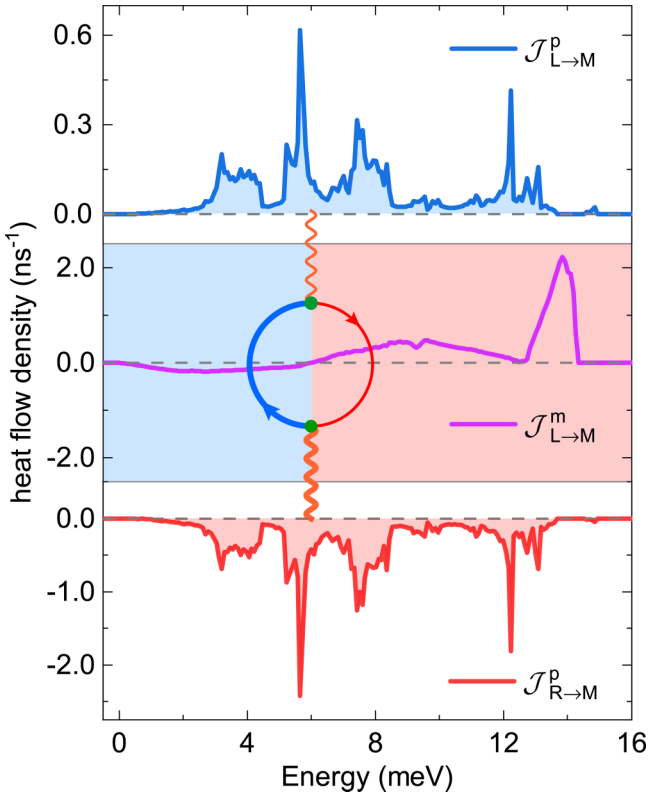
FIG. 7. Schematic for the micro-process of energy transfer from magnons to phonons in ferromagnetic/nonmagnetic (F/N) interfaces. A central temperature (T) of 50 K, a temperature difference (ΔT) of 1 K, and an external magnetic field (h_z) of 0.0 meV are adopted here. The thick lines in the diagrammatic representation of magnon-phonon scattering mean the accumulation of particles in the central region of the device, where magnons with higher energy ($\varepsilon > 6$ meV) transfer energy to phonons, and turn to be magnons with lower energy ($\varepsilon < 6$ meV).

on this point is held in Sec. III C. On the other hand, the magnetic atoms (Cr_3) mainly contribute to the high-frequency vibrations of phonons, while the low-frequency vibrations are mainly donated by the I atoms. However, the phonons with high energy are not involved in the MPS process, which further determines the weakness of the inelastic process. These results reveal the microprocess of energy exchange in the F/N interfaceand provide theoretical references for the selection of magnetic thermal functional materials.

C. Computational details and perspectives

In this subsection, we show the details of numerical computation as interfaced with first-principles calculations for further verification and study. Firstly, we talk about the computation of input parameters based on DFT. There are three essential parameters in the present NEGF formalism: the matrix elements of the Hamiltonian for magnons ($\mathcal{X}$), phonons ($\mathcal{K}$), and MPS ($\mathcal{M}$), which have been introduced in Sec. II A. More specifically, these three matrices are obtained from the Fourier transformation of X, K, and M, respectively [cf. Eqs. (A6), (A10), and (A15) in Appendix A], and all of them can be obtained from DFT calculations. The spin-polarized

DFT calculation was implemented in the open-source package OPENMX [82,83] using the generalized gradient approximation and Perdew-Burke-Ernzehof exchange-correlation functional [84]. An energy cutoff of 200 Ry was used, and a convergence threshold of 10^{-8} Hartree was adopted for each self-consistent step. First, a relaxation process of the primitive cell (8 atoms) ran with a **k** mesh of $8 \times 8 \times 1$ to obtain an optimized lattice constant of 6.985 Å until the interatomic forces were $<10^{-6}$ Hartree/Bohr. For the second-order force constants K, the finite displacement method as implemented in the PHONOPY [85] package was adopted on a supercell of $3 \times 3 \times 1$ unit cells (144 atoms). A **k** mesh of $2 \times 2 \times 1$ was used in the spin-polarized DFT calculation. For the matrix elements of the magnon Hamiltonian X, the evaluation of both the exchange coupling constants between each pair ($J_{i,j}$) and the magnetic moment of the atoms (S_i) are essential. In the present spin-polarized DFT calculations, the magnetic moments of Cr and I atoms are 3.4658 μ_B and -0.1575 μ_B, respectively, which agrees with previous studies. The Liechtenstein method [86] as implemented in our in-house code was adopted to evaluate the isotropic exchange coupling constants, and one can also use the built-in software in OPENMX. For the first-order magnon-phonon coupling matrix M, the finite displacement method based on Eq. (A13) in Appendix A was used. To reduce the cost of computing and improve the credibility of our data, a crystal symmetry correction was applied to these three matrix elements using the open-source package SPGLIB [87].

Once the three matrices $\mathcal{X}$, $\mathcal{K}$, and $\mathcal{M}$ were obtained, first, the initial Green's functions of magnons and phonons were computed via Eqs. (13) and (14). Afterwards, the self-consistent loop ran as based on Eqs. (15)–(22), until the average relative error of self-energies was $<10^{-9}$. A **k** (or **q**) mesh of $1 \times 47 \times 1$ and an energy sampling number of 959 were adopted to ensure the convergence of observables. In addition, it should be noted that the static modification contributed by first- and second-order SPC [77] to the dispersion of phonons was considered in our scheme since the spin-polarized DFT was adopted in the calculation of the second-order force constants K. The static part of first-order SPC contributes a static force to the magnetic atoms, while second-order SPC donates an additional modification to K directly, both of which were incorporated in the step of finite displacements. A similar treatment has been adopted in the case of electron-phonon scattering [70], where the static modification of the first- and second-order electron-phonon coupling to phonons was incorporated in the finite-displacement step. The consideration of MPS in our scheme is on the foundation of these modifications; thus, only the fluctuating part of the spin (magnons) needs to be considered.

The present NEGF formalism is mainly proposed to rigorously incorporate MPS into the quantum transport of a nanostructure with broken translation symmetry in the transport direction. In this way, it is possible to investigate transport behaviors of both magnons and phonons in magnetic nanostructures, especially in F/N interfaces, from a first-principles perspective. Moreover, the heat generation [69,75] of magnons in spin-wave devices is also an essential topic we need to further discuss, which has been glimpsed roughly in

Sec. III A. The tuning of heat/spin transport in strong MPS magnetic nanostructures across various means, such as gating [88] and twisting [89,90], also needs further investigation since strong scattering leads to strong nonlinear transport behaviors, and it is attractive for nanoscale magnetic thermal logic devices, such as magnetic heat/spin switches [79,91]. As this paper is mainly focused on the formalism determination and methodology development, further discussion of the above perspectives is pending in our future work.

IV. CONCLUSIONS

In summary, we propose a NEGF formalism and develop a method with first-principles input to rigorously incorporate MPS into the quantum heat transport of magnetic nanodevices. The theoretical formulation of self-energy of MPS is suggested through a diagrammatic perturbation analysis. Without the dependence on the 1D formalism, the present formalism naturally satisfies both the energy and momentum conservation in nanodevices with transverse periodicity. A generalized formalism of heat flow is proposed to distinguish the elastic and inelastic parts of energy exchange, which is also applicative for nanodevices with other kinds of scattering, such as electron-phonon and phonon-phonon scattering. The heat transport of magnons as dragged by phonons is evaluated in a magnetic nanodevice, based on CrI_3 ML, with an asymmetric spin configuration. The enhancement of thermal rectification and NDTC of magnons through the spin frozen phenomenon as manipulated by an external magnetic field is demonstrated, where the reduction of inelastic heat flow by six times is observed as the external magnetic field rises from 0 to 5 meV. The temperature deviation of magnons proposed in this paper is shown to be significant to evaluate the strength of the phonon drag effect. The present NEGF formalism paves the way for first-principles investigation of heat generation of magnons in spintronic devices and is expected to provide *ab initio* insights for the design of magnetic thermal nanodevices as well as spin-dependent thermoelectric nanodevices. In this paper, we thus open the gate to first-principles investigations of quantum heat transport in magnetic nanostructures and pave the way for the theoretical design of nanoscale magnetic thermal devices.

APPENDIX A: FORMALISM TRANSFORMATION OF THE HAMILTONIAN

The simplified model of a ferromagnetic insulator with a transverse periodicity on the yz plane is shown in Fig. 8. We assume both the spin-quantization axis and the external magnetic field h_z point along the $+z$ direction. The spin properties of such a system can be described by the Heisenberg spin
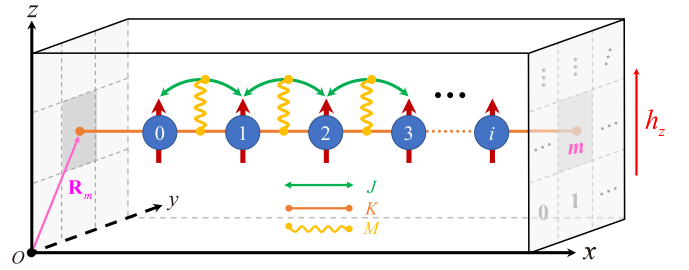
FIG. 8. Schematic of the simplified physical model for a three-dimensional (3D) ferromagnetic nanostructure with a transverse (yz plane) periodicity. An external magnetic (h_z) along the $+z$ direction is applied to the entire system. The straight lines connecting two atoms denote the force constants K, the curves with double-arrow between two spins denote exchange coupling constants J, and the wavy lines between J and K denote the magnon-phonon coupling constants M.

Hamiltonian as

$$\hat{\mathcal{H}}_{sp} = -\frac{1}{2}\sum_{m,n}\sum_{i,j}J_{i,j}(m,n)\hat{S}_{m,i}\cdot\hat{S}_{n,j} - h_z\sum_{m,i}\hat{S}_{m,i}^z, \quad \text{(A1)}$$

where m and n run over all the transverse cells along the yz plane, and i and j run over the spin-localized atoms in one cell. Here, $J_{i,j}(m,n)$ is the isotropic exchange coupling constant between two spins localized at the atoms labeled by (m,i) and (n,j). Also, $\hat{S}_{m,i}$ and $\hat{S}_{m,i}^z$ are the total and the z component of the spin operator, respectively. Applying the Holstein-Primakoff transformation to Eq. (A1) and retaining only the linear-order terms yields

$$\hat{\mathcal{H}}_{sp} = \sum_{m,n}\sum_{i,j}X_{i,j}(m,n)\hat{a}_{m,i}^+\hat{a}_{n,j}, \quad \text{(A2)}$$

and the matrix element $X_{i,j}(m,n)$ reads

$$X_{i,j}(m,n)|_{m,i\neq n,j} = -J_{i,j}(m,n)\sqrt{S_iS_j},$$

$$X_{i,i}(m,m) = h_z + \sum_{n,j\neq m,i}J_{i,j}(m,n)S_j, \quad \text{(A3)}$$

where $\hat{a}_i^+$ and $\hat{a}_i$ are the bosonic creation and annihilation operators of spin deviation (magnon), respectively, and S_i is the length of spin localized at the ith magnetic atom.

To serve in reciprocal space, we rewrite the magnon Hamiltonian through the following Fourier transformation:

$$\hat{a}_{m,i} = \frac{1}{\sqrt{N}}\sum_{\mathbf{k}}\hat{a}_{\mathbf{k},i}\exp(i\mathbf{k}\cdot\mathbf{R}_m), \quad \text{(A4)}$$

where $\mathbf{k} = (0, k_y, k_z)$ is the transverse wave vector of magnons. Here, $\mathbf{R}_m = (0, R_m^y, R_m^z)$ is the position vector of the mth cell on the yz plane, and thus, Eq. (A3) can be rewritten as

$$\hat{\mathcal{H}}_{sp} = \sum_{\mathbf{k}}\sum_{i,j}X_{i,j}(\mathbf{k})\hat{a}_{\mathbf{k},i}^\dagger\hat{a}_{\mathbf{k},j}, \quad \text{(A5)}$$

where the matrix element $X_{i,j}(\mathbf{k})$ reads

$$X_{i,j}(\mathbf{k}) = \sum_m X_{i,j}(m,0)\exp[-i\mathbf{k}\cdot(\mathbf{R}_m-\mathbf{R}_0)]. \quad \text{(A6)}$$

The phonon Hamiltonian in atomic representation reads

$$\hat{\mathcal{H}}_{ph} = \frac{1}{2} \sum_m \sum_i m_i \hat{\dot{u}}_{m,i} \hat{\dot{u}}_{m,i}$$
$$+ \frac{1}{2!} \sum_{m,n} \sum_{i,j} K_{i,j}(m,n) \hat{u}_{m,i} \hat{u}_{n,j}, \quad (A7)$$

where i and j run over all the vibrational degrees of freedom in one cell. Here, m_i is the atomic mass, and $K_{i,j}(m,n) = \frac{\partial^2 E}{\partial r_{m,i} \partial r_{n,j}}|_0$ is the second-order force constant. Also, $\hat{u}_{m,i}$ and $\hat{\dot{u}}_{m,i}$ are the displacement and velocity operators, respectively. For the same motivation with the spin system, we rewrite the phonon Hamiltonian through the following transformation:

$$\hat{u}_{m,i} = \frac{1}{\sqrt{N m_i}} \sum_{\mathbf{q}} \hat{u}_{\mathbf{q},i} \exp(i\mathbf{q} \cdot \mathbf{R}_m), \quad (A8)$$

where $\mathbf{q} = (0, q_y, q_z)$ is the transverse wave vector of phonons, and thus, Eq. (A7) is rewritten as

$$\hat{\mathcal{H}}_{ph} = \sum_{\mathbf{q}} \sum_{i,j} \mathcal{K}_{i,j}(\mathbf{q}) \hat{u}_{-\mathbf{q},i} \hat{u}_{\mathbf{q},j}, \quad (A9)$$

where $\hat{u}_{\mathbf{q},i}$ is the $\mathbf{q}$ component of $\hat{u}_{m,i}$, and the dynamical matrix $\mathcal{K}_{i,j}(\mathbf{q})$ reads

$$\mathcal{K}_{i,j}(\mathbf{q}) = \frac{1}{\sqrt{m_i m_j}} \sum_m K_{i,j}(m,0) \exp[-i\mathbf{q} \cdot (\mathbf{R}_m - \mathbf{R}_0)]. \quad (A10)$$

To incorporate MPS into the present NEGF framework, we assume the MPI to only originate from the lowest perturbation of atomic vibration $u_{m,i}$ to the exchange coupling constant $J_{i,j}(m,n)$, and thus, the MPS Hamiltonian in atomic representation reads

$$\hat{\mathcal{H}}_{sp-ph} = \sum_{m,n,l} \sum_{i,j,k} M_{i,j,k}(m,n,l) \hat{a}_{m,i}^+ \hat{a}_{n,j} \hat{u}_{l,k}, \quad (A11)$$

where $M_{i,j,k}(m,n,l)$ is the first-order SPC constant and is defined as

$$M_{i,j,k}(m,n,l) = \frac{\partial X_{i,j}(m,n)}{\partial r_{l,k}}\bigg|_0. \quad (A12)$$

To serve for the numerical calculation based on first-principles, we rewrite Eq. (A12) into a finite difference representation as

$$M_{i,j,k}(m,n,l) = \frac{X_{i,j}(m,n)|_{r_{l,k}+\delta} - X_{i,j}(m,n)|_{r_{l,k}-\delta}}{2\delta}, \quad (A13)$$

which is the so-called finite-displacement method since δ is the finite displacement of atom. Applying the transformation like the spin (or phonon) Hamiltonian in Eq. (A11) yields

$$\hat{\mathcal{H}}_{sp-ph} = \sum_{\mathbf{k},\mathbf{q}} \sum_{i,j,k} \mathcal{M}_{i,j,k}(\mathbf{k},\mathbf{q}) \hat{a}_{\mathbf{k},i}^\dagger \hat{a}_{\mathbf{k}-\mathbf{q},j} \hat{u}_{\mathbf{q},k}, \quad (A14)$$

where the conservation of momentum has been naturally satisfied since the summation of wave vectors of creation operators in Eq. (A14) is always equal to that of annihilation operators. The momentum-decomposed SPC constant $\mathcal{M}_{i,j,k}(\mathbf{k},\mathbf{q})$ reads

$$\mathcal{M}_{i,j,k}(\mathbf{k},\mathbf{q}) = \frac{1}{\sqrt{N m_k}} \sum_{m,n} M_{i,j,k}(m,n,0)$$

$$\times \exp[-i\mathbf{k} \cdot (\mathbf{R}_m - \mathbf{R}_0)]$$
$$\times \exp[i(\mathbf{k} - \mathbf{q}) \cdot (\mathbf{R}_n - \mathbf{R}_0)]. \quad (A15)$$

APPENDIX B: DERIVATION OF GREEN'S FUNCTIONS AND SELF-ENERGIES

We start from the definition of the contour-ordered Green's functions for magnons and phonons in 3D nanostructures. Transforming Eqs. (11) and (12) into the interaction picture yields

$$G_{i,j}(\mathbf{k}; \tau, \tau') = -\frac{i}{\hbar} \frac{\langle T_C[S_C \hat{a}_{\mathbf{k},i}(\tau) \hat{a}_{\mathbf{k},j}^\dagger(\tau')]\rangle_0}{\langle T_C S_C \rangle_0}, \quad (B1)$$

$$D_{i,j}(\mathbf{q}; \tau, \tau') = -\frac{i}{\hbar} \frac{\langle T_C[S_C \hat{u}_{\mathbf{q},i}(\tau) \hat{u}_{-\mathbf{q},j}(\tau')]\rangle_0}{\langle T_C S_C \rangle_0}, \quad (B2)$$

where $\langle \cdots \rangle_0$ denotes the expected value of the operator in the noninteracting ground state, and the time evolution operator S_C is defined as [92]

$$S_C = \exp\left[-\frac{i}{\hbar} \int_C d\tau \hat{\mathcal{H}}'(\tau)\right]$$
$$= \sum_{n=0}^{\infty} \frac{(-i/\hbar)^n}{n!} \int_C d\tau_1 \hat{\mathcal{H}}'(\tau_1) \cdots \int_C d\tau_n \hat{\mathcal{H}}'(\tau_n), \quad (B3)$$

where $\hat{\mathcal{H}}'$ is composed of the hopping term between the contacts and the central region, as well as the many-body term contributed by MPS. We only focus on the latter here since the former can be considered rigorously through Dyson's equation.

1. Unperturbed Green's functions

In the unperturbed case, both the MPS term of the Hamiltonian $\hat{\mathcal{H}}_{sp-ph}$ and the nonequilibrium potential from contacts are equal to $\hat{0}$, and thus, the system is actually in an equilibrium state. In this way, the unperturbed Green's functions of magnons and phonons can be produced from Eqs. (B1) and (B2) as

$$G_{i,j}^{(0)}(\mathbf{k}; \tau, \tau') = -\frac{i}{\hbar} \langle T_C[\hat{a}_{\mathbf{k},i}(\tau) \hat{a}_{\mathbf{k},j}^\dagger(\tau')]\rangle_0, \quad (B4)$$

$$D_{i,j}^{(0)}(\mathbf{q}; \tau, \tau') = -\frac{i}{\hbar} \langle T_C[\hat{u}_{\mathbf{q},i}(\tau) \hat{u}_{-\mathbf{q},j}(\tau')]\rangle_0, \quad (B5)$$

respectively. To relate the unperturbed Green's functions with the noninteracting Hamiltonian matrix elements, for instance, the contour-ordered Green function of the phonon can be decomposed into four-interrelated real-time Green's functions:

$$D_{i,j}^{(0),>}(\mathbf{q}; t, t') = -\frac{i}{\hbar} \langle \hat{u}_{\mathbf{q},i}(t) \hat{u}_{-\mathbf{q},j}(t')\rangle_0, \quad (B6)$$

$$D_{i,j}^{(0),<}(\mathbf{q}; t, t') = -\frac{i}{\hbar} \langle \hat{u}_{-\mathbf{q},j}(t') \hat{u}_{\mathbf{q},i}(t)\rangle_0, \quad (B7)$$

$$D_{i,j}^{(0),R}(\mathbf{q}; t, t') = -\frac{i}{\hbar} \theta(t - t') \langle [\hat{u}_{\mathbf{q},i}(t), \hat{u}_{-\mathbf{q},j}(t')]\rangle_0, \quad (B8)$$

$$D_{i,j}^{(0),A}(\mathbf{q}; t, t') = +\frac{i}{\hbar} \theta(t' - t) \langle [\hat{u}_{\mathbf{q},i}(t), \hat{u}_{-\mathbf{q},j}(t')]\rangle_0. \quad (B9)$$

Since in the equilibrium state the physical quantity only depends on the time difference, we transform Eqs. (B6)–(B9) into the frequency domain as

$$
\begin{aligned}
D_{i,j}^{(0),>}&(\mathbf{q}, \omega) \\
&= -2\pi i \sum_{\lambda} \frac{\phi_{\mathbf{q},\lambda;i}\phi_{\mathbf{q},\lambda;j}^{*}}{2\omega_{\mathbf{q},\lambda}}[(1 + n_{\mathbf{q},\lambda})\delta(\omega - \omega_{\mathbf{q},\lambda}) \\
&\quad + n_{\mathbf{q},\lambda}\delta(\omega + \omega_{\mathbf{q},\lambda})],
\end{aligned}
\tag{B10}
$$

$$
\begin{aligned}
D_{i,j}^{(0),<}&(\mathbf{q}, \omega) \\
&= -2\pi i \sum_{\lambda} \frac{\phi_{\mathbf{q},\lambda;i}\phi_{\mathbf{q},\lambda;j}^{*}}{2\omega_{\mathbf{q},\lambda}}[(1 + n_{\mathbf{q},\lambda})\delta(\omega + \omega_{\mathbf{q},\lambda}) \\
&\quad + n_{\mathbf{q},\lambda}\delta(\omega - \omega_{\mathbf{q},\lambda})],
\end{aligned}
\tag{B11}
$$

$$
\begin{aligned}
D_{i,j}^{(0),R}&(\mathbf{q}, \omega) \\
&= \sum_{\lambda} \frac{\phi_{\mathbf{q},\lambda;i}\phi_{\mathbf{q},\lambda;j}^{*}}{2\omega_{\mathbf{q},\lambda}}\left(\frac{1}{\omega - \omega_{\mathbf{q},\lambda} + i\eta} - \frac{1}{\omega + \omega_{\mathbf{q},\lambda} + i\eta}\right),
\end{aligned}
\tag{B12}
$$

$$
\begin{aligned}
D_{i,j}^{(0),A}&(\mathbf{q}, \omega) \\
&= \sum_{\lambda} \frac{\phi_{\mathbf{q},\lambda;i}\phi_{\mathbf{q},\lambda;j}^{*}}{2\omega_{\mathbf{q},\lambda}}\left(\frac{1}{\omega - \omega_{\mathbf{q},\lambda} - i\eta} - \frac{1}{\omega + \omega_{\mathbf{q},\lambda} - i\eta}\right),
\end{aligned}
\tag{B13}
$$

where * denotes the complex conjugate, and $n_{\mathbf{q},\lambda}$ is the occupation number of phonons with wave vector $\mathbf{q}$ at mode λ. Here, $\theta(t)$ and $\delta(\omega)$ are the Heaviside step function and Dirac delta function, respectively, while η is a positive infinitesimal. These four Green's functions, among which only one is independent, are interrelated via the following relations:

$$
D_{i,j}^{(0),A}(\mathbf{q}, \omega) = \left[D_{j,i}^{(0),R}(\mathbf{q}, \omega)\right]^{*},
\tag{B14}
$$

$$
D_{i,j}^{(0),<}(\mathbf{q}, \omega) = f_{B}(\omega)\left[D_{i,j}^{(0),R}(\mathbf{q}, \omega) - D_{i,j}^{(0),A}(\mathbf{q}, \omega)\right],
\tag{B15}
$$

$$
D_{i,j}^{(0),>}(\mathbf{q}, \omega) = [1 + f_{B}(\omega)]\left[D_{i,j}^{(0),R}(\mathbf{q}, \omega) - D_{i,j}^{(0),A}(\mathbf{q}, \omega)\right],
\tag{B16}
$$

while the retarded Green function $D_{i,j}^{(0),R}(\mathbf{q}, \omega)$ is related with the dynamical matrix $\mathcal{K}(\mathbf{q})$ via the following:

$$
\mathbf{D}^{(0),R}(\mathbf{q}, \omega) = [(\omega + i\eta)^{2}\mathbf{I} - \mathcal{K}(\mathbf{q})]^{-1},
\tag{B17}
$$

where $f_{B}(\omega)$ is the Bose-Einstein distribution function. The other three unperturbed Green's functions thus can also be rewritten as

$$
\mathbf{D}^{(0),A}(\mathbf{q}, \omega) = [\mathbf{D}^{(0),R}(\mathbf{q}, \omega)]^{\dagger},
\tag{B18}
$$

$$
\mathbf{D}^{(0),<}(\mathbf{q}, \omega) = f_{B}(\omega)[\mathbf{D}^{(0),R}(\mathbf{q}, \omega) - \mathbf{D}^{(0),A}(\mathbf{q}, \omega)],
\tag{B19}
$$

$$
\mathbf{D}^{(0),>}(\mathbf{q}, \omega) = [1 + f_{B}(\omega)][\mathbf{D}^{(0),R}(\mathbf{q}, \omega) - \mathbf{D}^{(0),A}(\mathbf{q}, \omega)],
\tag{B20}
$$

where $\dagger$ means conjugate transpose. Analogous to the derivation of the phonon Green's functions, the unperturbed Green's functions of magnons in matrix representation are given by

$$
\mathbf{G}^{(0),R}(\mathbf{k}, \varepsilon) = [(\varepsilon + i\eta)\mathbf{I} - \mathcal{X}(\mathbf{k})]^{-1},
\tag{B21}
$$

$$
\mathbf{G}^{(0),A}(\mathbf{k}, \varepsilon) = [\mathbf{G}^{(0),R}(\mathbf{k}, \varepsilon)]^{\dagger},
\tag{B22}
$$

$$
\mathbf{G}^{(0),<}(\mathbf{k}, \varepsilon) = f_{B}(\varepsilon)[\mathbf{G}^{(0),R}(\mathbf{k}, \varepsilon) - \mathbf{G}^{(0),A}(\mathbf{k}, \varepsilon)],
\tag{B23}
$$

$$
\mathbf{G}^{(0),>}(\mathbf{k}, \varepsilon) = [1 + f_{B}(\varepsilon)][\mathbf{G}^{(0),R}(\mathbf{k}, \varepsilon) - \mathbf{G}^{(0),A}(\mathbf{k}, \varepsilon)].
\tag{B24}
$$

2. Perturbed Green's functions and self-energies for MPS

To produce the perturbed Green's functions, the high-order terms of S_{C} need to be concerned. Since the odd terms of Eq. (B3) are vanishing due to containing an odd number of displacement operators, the perturbed Green function keeping only the lowest two nonzero terms of the magnon system reads

$$
G_{i,j}(\mathbf{k}; \tau, \tau') = G_{i,j}^{(0)}(\mathbf{k}; \tau, \tau') + G_{i,j}^{(2)}(\mathbf{k}; \tau, \tau'),
\tag{B25}
$$

which is the so-called Born approximation (BA), and the second-order term is defined as

$$
\begin{aligned}
G_{i,j}^{(2)}(\mathbf{k}; \tau, \tau') &= \frac{1}{2!}\left(\frac{-i}{\hbar}\right)^{3}\int_{C} d\tau_{1} \\
&\quad \times \int_{C} d\tau_{2}\langle T_{C}[\hat{H}'(\tau_{1})\hat{H}'(\tau_{2})\hat{a}_{\mathbf{k},i}(\tau)\hat{a}_{\mathbf{k},j}^{\dagger}(\tau')]\rangle_{0}.
\end{aligned}
\tag{B26}
$$

Only the connected diagrams are considered because of the exact canceling of disconnected diagrams in the expansion of $G_{i,j}(\mathbf{k}; \tau, \tau')$ by the vacuum polarization diagrams from $\langle T_{C}S_{C}\rangle_{0}$. Substituting Eq. (A14) into Eq. (B26) and applying Wick's theorem [93] yields two topologically unequal connections:

$$
G_{i,j}^{(2)}(\mathbf{k}; \tau, \tau') = G_{i,j}^{(2),H}(\mathbf{k}; \tau, \tau') + G_{i,j}^{(2),F}(\mathbf{k}; \tau, \tau'),
\tag{B27}
$$

where the first term is the so-called Hartree term and reads

$$
\begin{aligned}
G_{i,j}^{(2),H}&(\mathbf{k}; \tau, \tau') \\
&= i\hbar \int_{C} d\tau_{1}\int_{C} d\tau_{2}G_{i,i_{1}}^{(0)}(\mathbf{k}; \tau, \tau_{1})G_{j_{1},j}^{(0)}(\mathbf{k}; \tau_{1}, \tau') \\
&\quad \times \sum_{\mathbf{k}'}\mathcal{M}_{i_{1},j_{1},k_{1}}(\mathbf{k}, \mathbf{0})\mathcal{M}_{i_{2},j_{2},k_{2}}(\mathbf{k}', \mathbf{0}) \\
&\quad \times G_{j_{2},i_{2}}^{(0)}(\mathbf{k}'; \tau_{2}, \tau_{2})D_{k_{1},k_{2}}^{(0)}(\mathbf{0}; \tau_{1}, \tau_{2}),
\end{aligned}
\tag{B28}
$$

while the Forck term $G_{i,j}^{(2),F}$ reads

$$
\begin{aligned}
G_{i,j}^{(2),F}&(\mathbf{k}; \tau, \tau') \\
&= i\hbar \int_{C} d\tau_{1}\int_{C} d\tau_{2}G_{i,i_{1}}^{(0)}(\mathbf{k}; \tau, \tau_{1})G_{j_{2},j}^{(0)}(\mathbf{k}; \tau_{2}, \tau') \\
&\quad \times \sum_{\mathbf{q}}\mathcal{M}_{i_{1},j_{1},k_{1}}(\mathbf{k}, \mathbf{q})\mathcal{M}_{i_{2},j_{2},k_{2}}(\mathbf{k} - \mathbf{q}, -\mathbf{q}) \\
&\quad \times G_{j_{1},i_{2}}^{(0)}(\mathbf{k} - \mathbf{q}; \tau_{1}, \tau_{2})D_{k_{1},k_{2}}^{(0)}(\mathbf{q}; \tau_{1}, \tau_{2}),
\end{aligned}
\tag{B29}
$$

where the Einstein summation convention is adopted, and the expansion coefficient $\frac{1}{2!}$ in Eq. (B26) is canceled by the swap equivalence of τ_{1} and τ_{2}, as shown in Fig. 9. Since the Hartree term in Eq. (B28) is ignored, we only focus on the Forck term. Comparing the second-order Green function of the Forck term in Eq. (B29) with Dyson's equation [92,93] and adopting the
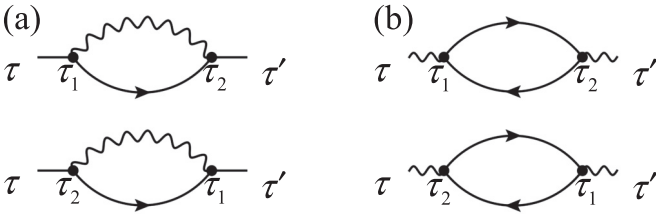
FIG. 9. The equivalent connections for the magnon-phonon scattering self-energy of (a) magnons and (b) phonons. The exchange of τ_1 and τ_2 produces two equivalent connected diagrams and cancels the second-order expansion coefficient $(\frac{1}{2!})$ of time evolution operator S_C.

SCBA [53,73] yields the MPS self-energy of magnons as

$$
\Sigma_{i_1,j_2}(\mathbf{k};\tau_1,\tau_2)
$$
$$
= i\hbar \sum_{\mathbf{q}} \mathcal{M}_{i_1,j_1,k_1}(\mathbf{k},\mathbf{q})\mathcal{M}_{i_2,j_2,k_2}(\mathbf{k}-\mathbf{q},-\mathbf{q})
$$
$$
\times G_{j_1,i_2}(\mathbf{k}-\mathbf{q};\tau_1,\tau_2)D_{k_1,k_2}(\mathbf{q};\tau_1,\tau_2). \quad \text{(B30)}
$$

Due to the convenience of serving on the real-time domain, we apply the analytical continuation technology based on the Langreth theorem [92] to Eq. (B30), and the real-time expression of the greater/lesser self-energy is found to be

$$
\Sigma_{i_1,j_2}^{>,<}(\mathbf{k};t_1,t_2)
$$
$$
= i\hbar \sum_{\mathbf{q}} \mathcal{M}_{i_1,j_1,k_1}(\mathbf{k},\mathbf{q})\mathcal{M}_{i_2,j_2,k_2}(\mathbf{k}-\mathbf{q},-\mathbf{q})
$$
$$
\times G_{j_1,i_2}^{>,<}(\mathbf{k}-\mathbf{q};t_1,t_2)D_{k_1,k_2}^{>,<}(\mathbf{q};t_1,t_2), \quad \text{(B31)}
$$

where t_1 and t_2 are real time from $-\infty$ to $+\infty$, and the retarded one reads

$$
\Sigma_{i_1,j_2}^{R}(\mathbf{k};t_1,t_2)
$$
$$
= i\hbar \sum_{\mathbf{q}} \mathcal{M}_{i_1,j_1,k_1}(\mathbf{k},\mathbf{q})\mathcal{M}_{i_2,j_2,k_2}(\mathbf{k}-\mathbf{q},-\mathbf{q})
$$
$$
\times \big[G_{j_1,i_2}^{R}(\mathbf{k}-\mathbf{q};t_1,t_2)D_{k_1,k_2}^{>}(\mathbf{q};t_1,t_2)
$$
$$
+ G_{j_1,i_2}^{<}(\mathbf{k}-\mathbf{q};t_1,t_2)D_{k_1,k_2}^{R}(\mathbf{q};t_1,t_2) \big]. \quad \text{(B32)}
$$

For steady state transport problems, we transform the double-time physical quantity to the frequency domain since it only relates to the time difference $t_1 - t_2$. The frequency-dependent self-energy of magnons reads

$$
\Sigma_{i_1,j_2}^{>,<}(\mathbf{k},\varepsilon)
$$
$$
= i\hbar \sum_{\mathbf{q}} \mathcal{M}_{i_1,j_1,k_1}(\mathbf{k},\mathbf{q})\mathcal{M}_{i_2,j_2,k_2}(\mathbf{k}-\mathbf{q},-\mathbf{q})
$$
$$
\times \int_{-\infty}^{+\infty} \frac{d\omega}{2\pi} G_{j_1,i_2}^{>,<}(\mathbf{k}-\mathbf{q},\varepsilon-\hbar\omega)D_{k_1,k_2}^{>,<}(\mathbf{q},\omega), \quad \text{(B33)}
$$
$$
\Sigma_{i_1,j_2}^{R}(\mathbf{k},\varepsilon) = i\hbar \sum_{\mathbf{q}} \mathcal{M}_{i_1,j_1,k_1}(\mathbf{k},\mathbf{q})\mathcal{M}_{i_2,j_2,k_2}(\mathbf{k}-\mathbf{q},-\mathbf{q})
$$
$$
\times \int_{-\infty}^{+\infty} \frac{d\omega}{2\pi} \big[G_{j_1,i_2}^{R}(\mathbf{k}-\mathbf{q},\varepsilon-\hbar\omega)D_{k_1,k_2}^{>}(\mathbf{q},\omega)
$$
$$
+ G_{j_1,i_2}^{<}(\mathbf{k}-\mathbf{q},\varepsilon-\hbar\omega)D_{k_1,k_2}^{R}(\mathbf{q},\omega) \big], \quad \text{(B34)}
$$

and the full Green's functions of magnons in the frequency domain are given by Dyson's equation and the Keldysh formulation [64] as

$$
\mathbf{G}^{R}(\mathbf{k},\varepsilon) = [\mathbf{G}^{(0),R}(\mathbf{k},\varepsilon)^{-1} - \boldsymbol{\Sigma}^{R}(\mathbf{k},\varepsilon)]^{-1}, \quad \text{(B35)}
$$

$$
\mathbf{G}^{>,<}(\mathbf{k},\varepsilon) = \mathbf{G}^{R}(\mathbf{k},\varepsilon)\boldsymbol{\Sigma}^{>,<}(\mathbf{k},\varepsilon)\mathbf{G}^{A}(\mathbf{k},\varepsilon), \quad \text{(B36)}
$$

where $\boldsymbol{\Sigma} = \boldsymbol{\Sigma}_T + \boldsymbol{\Sigma}_M$ is the total self-energy, and $\boldsymbol{\Sigma}_T$ is the self-energy donated by the semi-infinite thermal contacts, while $\boldsymbol{\Sigma}_M$ is the matrix notation of the MPS self-energy. Unlike the case in recent studies [38,39] about anharmonic phonon transport, Eqs. (B33)–(B36) cannot build a set of self-consistent equations since the undetermined full Green function of phonons $D_{i,j}(\mathbf{q},\omega)$ is contained in the many-body self-energy of magnons.

We follow the above derivation process of the many-body Green's functions of magnons, and the many-body self-energy of phonons under SCBA is found to be

$$
\Pi_{k_1,k_2}(\mathbf{q};\tau_1,\tau_2)
$$
$$
= i\hbar \sum_{\mathbf{k}} \mathcal{M}_{i_1,j_1,k_1}(\mathbf{k}-\mathbf{q},-\mathbf{q})\mathcal{M}_{i_2,j_2,k_2}(\mathbf{k},\mathbf{q})
$$
$$
\times G_{j_1,i_2}(\mathbf{k};\tau_1,\tau_2)G_{j_2,i_1}(\mathbf{k}-\mathbf{q};\tau_2,\tau_1). \quad \text{(B37)}
$$

It should be noted that, as distinguished from the magnon system, there is only one irreducible connected diagram contributing the lowest-order scattering to the phonon system. Apply the analytical continuation to Eq. (B37), and the final expressions of the self-energies of phonons in the frequency domain are

$$
\Pi_{k_1,k_2}^{>,<}(\mathbf{q},\omega) = i \sum_{\mathbf{k}} \mathcal{M}_{i_1,j_1,k_1}(\mathbf{k}-\mathbf{q},-\mathbf{q})\mathcal{M}_{i_2,j_2,k_2}(\mathbf{k},\mathbf{q})
$$
$$
\times \int_{-\infty}^{+\infty} \frac{d\varepsilon}{2\pi} G_{j_1,i_2}^{>,<}(\mathbf{k},\varepsilon)G_{j_2,i_1}^{<,>}(\mathbf{k}-\mathbf{q},\varepsilon-\hbar\omega), \quad \text{(B38)}
$$

$$
\Pi_{k_1,k_2}^{R}(\mathbf{q},\omega) = i \sum_{\mathbf{k}} \mathcal{M}_{i_1,j_1,k_1}(\mathbf{k}-\mathbf{q},-\mathbf{q})\mathcal{M}_{i_2,j_2,k_2}(\mathbf{k},\mathbf{q})
$$
$$
\times \int_{-\infty}^{+\infty} \frac{d\varepsilon}{2\pi} \big[G_{j_1,i_2}^{R}(\mathbf{k},\varepsilon)G_{j_2,i_1}^{<}(\mathbf{k}-\mathbf{q},\varepsilon-\hbar\omega)
$$
$$
+ G_{j_1,i_2}^{<}(\mathbf{k},\varepsilon)G_{j_2,i_1}^{A}(\mathbf{k}-\mathbf{q},\varepsilon-\hbar\omega) \big], \quad \text{(B39)}
$$

and the matrix notation of the full phonon Green function in the frequency domain reads

$$
\mathbf{D}^{R}(\mathbf{q},\omega) = [\mathbf{D}^{(0),R}(\mathbf{q},\omega)^{-1} - \boldsymbol{\Pi}^{R}(\mathbf{q},\omega)]^{-1}, \quad \text{(B40)}
$$
$$
\mathbf{D}^{>,<}(\mathbf{q},\omega) = \mathbf{D}^{R}(\mathbf{q},\omega)\boldsymbol{\Pi}^{>,<}(\mathbf{q},\omega)\mathbf{D}^{A}(\mathbf{q},\omega). \quad \text{(B41)}
$$

The full Green's functions of magnons as well as phonons can be calculated iteratively through Eqs. (B33)–(B36) and (B38)–(B41). Once the numerical values of scattering self-energies are converged, the observables, such as heat flow and LDOS, can be obtained.

APPENDIX C: DISPERSION RELATIONS AND HEAT FLOWS

The dispersion relations of the magnon and phonon along the transverse direction are shown in Fig. 10(a). It is seen that the maximum energy of phonons ($\sim$30 meV) is about twice the maximum energy of magnons ($\sim$15 meV). Due to the energy conservation in the MPS process, the phonons with higher energy ($\hbar\omega > 15$ meV) are forbidden to participate in the MPS process. Figure 10(b) shows the temperature dependence of (elastic and inelastic) heat flows with and without MPS. The parameter settings are the same as that in Fig. 5(a). It is seen that the elastic heat flow ($\mathcal{I}^p_{L\to R}$) of phonons is far greater than the inelastic one ($\mathcal{I}^p_{L\to M}$), which indicates that MPS in the present F/N interface based on CrI$_3$ ML is weak but still cannot be ignored at high temperature ($T > 100$ K). These results suggest that a great thermal rectification or NDTC could be observed in magnetic nanostructures with weak bounding, such as van der Waals interfaces, where the contribution of phonons to elastic heat transport is quite small.
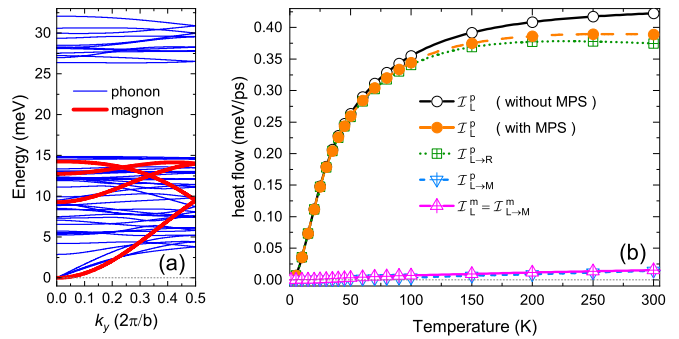
FIG. 10. (a) The dispersion relations of magnon (thin solid lines) and phonon (bold solid lines) along the transverse direction (*y*-axis); phonons with higher energy ($\hbar\omega > 15$ meV) are forbidden to participate in the MPS process; (b) the temperature dependence of heat flow without (hollow circle) and with MPS (others); a temperature difference of 1 K is adopted and an external magnetic field of 0.0 meV is used; MPS impedes phonon transport obviously at high temperature.

[1] D. G. Cahill, P. V. Braun, G. Chen, D. R. Clarke, S. Fan, K. E. Goodson, P. Keblinski, W. P. King, G. D. Mahan, A. Majumdar, H. J. Maris, S. R. Phillpot, E. Pop, and L. Shi, Nanoscale thermal transport. II. 2003–2012, Appl. Phys. Rev. **1**, 011305 (2014).

[2] A. J. Minnich, M. S. Dresselhaus, Z. F. Ren, and G. Chen, Bulk nanostructured thermoelectric materials: current research and future prospects, Energy Environ. Sci. **2**, 466 (2009).

[3] M. Zebarjadi, K. Esfarjani, M. S. Dresselhaus, Z. F. Ren, and G. Chen, Perspectives on thermoelectrics: From fundamentals to device applications, Energy Environ. Sci. **5**, 5147 (2012).

[4] N. Li, J. Ren, L. Wang, G. Zhang, P. Hänggi, and B. Li, Colloquium: Phononics: Manipulating heat flow with electronic analogs and beyond, Rev. Mod. Phys. **84**, 1045 (2012).

[5] G. Wehmeyer, T. Yabuki, C. Monachon, J. Wu, and C. Dames, Thermal diodes, regulators, and switches: Physical mechanisms and potential applications, Appl. Phys. Rev. **4**, 041304 (2017).

[6] K. Schwab, E. A. Henriksen, J. M. Worlock, and M. L. Roukes, Measurement of the quantum of thermal conductance, Nature (London) **404**, 974 (2000).

[7] J. M. Ziman, *Electrons and Phonons: The Theory of Transport Phenomena in Solids* (Oxford University Press, Oxford, 2001).

[8] G. Chen, *Nanoscale Energy Transport and Conversion: A Parallel Treatment of Electrons, Molecules, Phonons, and Photons* (Oxford University Press, Oxford, 2005).

[9] I. Žutić, J. Fabian, and S. D. Sarma, Spintronics: fundamentals and applications, Rev. Mod. Phys. **76**, 323 (2004).

[10] A. V. Chumak, V. I. Vasyuchka, A. A. Serga, and B. Hillebrands, Magnon spintronics, Nat. Phys. **11**, 453 (2015).

[11] G. E. Bauer, E. Saitoh, and B. J. Van Wees, Spin caloritronics, Nat. Mater. **11**, 391 (2012).

[12] S. R. Boona, R. C. Myers, and J. P. Heremans, Spin caloritronics, Energy Environ. Sci. **7**, 885 (2014).

[13] M. Montagnese, M. Otter, X. Zotos, D. A. Fishman, N. Hlubek, O. Mityashkin, C. Hess, R. Saint-Martin, S. Singh, A. Revcolevschi, and P. H. M. van Loosdrecht, Phonon-Magnon

Interaction in Low Dimensional Quantum Magnets Observed by Dynamic Heat Transport Measurements, Phys. Rev. Lett. **110**, 147206 (2013).

[14] S. R. Boona and J. P. Heremans, Magnon thermal mean free path in yttrium iron garnet, Phys. Rev. B **90**, 064421 (2014).

[15] G. T. Hohensee, R. B. Wilson, J. P. Feser, and D. G. Cahill, Magnon-phonon coupling in the spin-ladder compound Ca$_9$La$_5$Cu$_{24}$O$_{41}$ measured by time-domain thermoreflectance, Phys. Rev. B **89**, 024422 (2014).

[16] K. Uchida, S. Takahashi, K. Harii, J. Ieda, W. Koshibae, K. Ando, S. Maekawa, and E. Saitoh, Observation of the spin Seebeck effect, Nature (London) **455**, 778 (2008).

[17] K. Uchida, H. Adachi, T. An, T. Ota, M. Toda, B. Hillebrands, S. Maekawa, and E. Saitoh, Long-range spin Seebeck effect and acoustic spin pumping, Nat. Mater. **10**, 737 (2011).

[18] K. Uchida, H. Adachi, T. An, H. Nakayama, M. Toda, B. Hillebrands, S. Maekawa, and E. Saitoh, Acoustic spin pumping: direct generation of spin currents from sound waves in Pt/Y$_3$Fe$_5$O$_{12}$ hybrid structures, J. Appl. Phys. **111**, 053903 (2012).

[19] M. Weiler, H. Huebl, F. S. Goerg, F. D. Czeschka, R. Gross, and S. T. B. Goennenwein, Spin Pumping with Coherent Elastic Waves, Phys. Rev. Lett. **108**, 176601 (2012).

[20] T. Kikkawa, K. Shen, B. Flebus, R. A. Duine, K. I. Uchida, Z. Qiu, G. E. W. Bauer, and E. Saitoh, Magnon Polarons in the Spin Seebeck Effect, Phys. Rev. Lett. **117**, 207203 (2016).

[21] L. J. Cornelissen, K. Oyanagi, T. Kikkawa, Z. Qiu, T. Kuschel, G. E. W. Bauer, B. J. van Wees, and E. Saitoh, Nonlocal magnon-polaron transport in yttrium iron garnet, Phys. Rev. B **96**, 104441 (2017).

[22] G. Go, S. K. Kim, and K. J. Lee, Topological Magnon-Phonon Hybrid Excitations in Two-Dimensional Ferromagnets with Tunable Chern Numbers, Phys. Rev. Lett. **123**, 237207 (2019).

[23] M. Akazawa, M. Shimozawa, S. Kittaka, T. Sakakibara, R. Okuma, Z. Hiroi, H. Y. Lee, N. Kawashima, J. H. Han, and M. Yamashita, Thermal Hall Effects of Spins and Phonons

in Kagome Antiferromagnet Cd-Kapellasite, Phys. Rev. X **10**, 041059 (2020).

[24] Y. Li, Z. Yamani, Y. Song, W. Wang, C. Zhang, D. W. Tam, T. Chen, D. Hu, Z. Xu, S. Chi, K. Xia, L. Zhang, S. Cui, W. Guo, Z. Fang, Y. Liu, and P. Dai, Dynamic Spin-Lattice Coupling and Nematic Fluctuations in NaFeAs, Phys. Rev. X **8**, 021056 (2018).

[25] J. Flipse, F. K. Dejene, D. Wagenaar, G. E. W. Bauer, J. Ben Youssef, and B. J. Van Wees, Observation of the Spin Peltier Effect for Magnetic Insulators, Phys. Rev. Lett. **113**, 027601 (2014).

[26] E. J. Guo, J. Cramer, A. Kehlberger, C. A. Ferguson, D. A. MacLaren, G. Jakob, and M. Kläui, Influence of Thickness and Interface on the Low-Temperature Enhancement of the Spin Seebeck Effect in YIG Films, Phys. Rev. X **6**, 031012 (2016).

[27] W. G. Yang and H. Schmidt, Acoustic control of magnetism toward energy-efficient applications, Appl. Phys. Rev. **8**, 021304 (2021).

[28] S. Baroni, S. De Gironcoli, A. Dal Corso, and P. Giannozzi, Phonons and related crystal properties from density-functional perturbation theory, Rev. Mod. Phys. **73**, 515 (2001).

[29] F. Giustino, Electron-phonon interactions from first principles, Rev. Mod. Phys. **89**, 015003 (2017).

[30] W. Li, J. Carrete, N. A. Katcho, and N. Mingo, SHENGBTE: a solver of the Boltzmann transport equation for phonons, Comput. Phys. Commun. **185**, 1747 (2014).

[31] J. Zhou, B. Liao, and G. Chen, First-principles calculations of thermal, electrical, and thermoelectric transport properties of semiconductors, Semicond. Sci. Technol. **31**, 043001 (2016).

[32] T. Feng and X. Ruan, Four-phonon scattering reduces intrinsic thermal conductivity of graphene and the contributions from flexural phonons, Phys. Rev. B **97**, 045202 (2018).

[33] K. Q. Chen, W. X. Li, W. Duan, Z. Shuai, and B. L. Gu, Effect of defects on the thermal conductivity in a nanowire, Phys. Rev. B **72**, 045422 (2005).

[34] X.-F. Peng, K.-Q. Chen, Q. Wan, B. S. Zou, and W. Duan, Quantized thermal conductance at low temperatures in quantum wire with catenoidal contacts, Phys. Rev. B **81**, 195317 (2010).

[35] Y. Xu, J. S. Wang, W. Duan, B. L. Gu, and B. Li, Nonequilibrium Green's function method for phonon-phonon interactions and ballistic-diffusive thermal transport, Phys. Rev. B **78**, 224303 (2008).

[36] J. T. Lü, R. B. Christensen, G. Foti, T. Frederiksen, T. Gunst, and M. Brandbyge, Efficient calculation of inelastic vibration signals in electron transport: Beyond the wide-band approximation, Phys. Rev. B **89**, 081405(R) (2014).

[37] Y. Lee, M. Bescond, D. Logoteta, N. Cavassilas, M. Lannoo, and M. Luisier, Anharmonic phonon-phonon scattering modeling of three-dimensional atomistic transport: An efficient quantum treatment, Phys. Rev. B **97**, 205447 (2018).

[38] J. Dai and Z. Tian, Rigorous formalism of anharmonic atomistic Green's function for three-dimensional interfaces, Phys. Rev. B **101**, 041301(R) (2020).

[39] Y. Guo, M. Bescond, Z. Zhang, M. Luisier, M. Nomura, and S. Volz, Quantum mechanical modeling of anharmonic phonon-phonon scattering in nanostructures, Phys. Rev. B **102**, 195412 (2020).

[40] B. Liao, J. Zhou, and G. Chen, Generalized Two-Temperature Model for Coupled Phonon-Magnon Diffusion, Phys. Rev. Lett. **113**, 025902 (2014).

[41] R. Schmidt, F. Wilken, T. S. Nunner, and P. W. Brouwer, Boltzmann approach to the longitudinal spin Seebeck effect, Phys. Rev. B **98**, 134421 (2018).

[42] X. Wu, Z. Liu, and T. Luo, Magnon and phonon dispersion, lifetime, and thermal conductivity of iron from spin-lattice dynamics simulations, J. Appl. Phys. **123**, 085109 (2018).

[43] J. Hellsvik, D. Thonig, K. Modin, D. Iuşan, A. Bergman, O. Eriksson, L. Bergqvist, and A. Delin, General method for atomistic spin-lattice dynamics with first-principles accuracy, Phys. Rev. B **99**, 104302 (2019).

[44] F. Körmann, B. Grabowski, B. Dutta, T. Hickel, L. Mauger, B. Fultz, and J. Neugebauer, Temperature Dependent Magnon-Phonon Coupling in bcc Fe from Theory and Experiment, Phys. Rev. Lett. **113**, 165503 (2014).

[45] B. H. Zhang, Y. S. Hou, Z. Wang, and R. Q. Wu, First-principles studies of spin-phonon coupling in monolayer $Cr_2Ge_2Te_6$, Phys. Rev. B **100**, 224427 (2019).

[46] K. Wang, X. Xu, Y. Cheng, M. Zhang, J. S. Wang, H. Wang, and G. Zhang, Magnon relaxation time in ferromagnetic $Cr_2Ge_2Te_6$ monolayer governed by magnon-phonon interaction, Appl. Phys. Lett. **118**, 023102 (2021).

[47] Y. Y. Liu, B. L. Li, S. Z. Chen, X. Jiang, and K. Q. Chen, Effect of room temperature lattice vibration on the electron transport in graphene nanoribbons, Appl. Phys. Lett. **111**, 133107 (2017).

[48] Y. Xu, X. Chen, J.-S. Wang, B.-L. Gu, and W. Duan, Thermal transport in graphene junctions and quantum dots, Phys. Rev. B **81**, 195425 (2010).

[49] L. Zhang, J. S. Wang, and B. Li, Ballistic thermal rectification in nanoscale three-terminal junctions, Phys. Rev. B **81**, 100301(R) (2010).

[50] Z. Q. Zhang and J. T. Lü, Thermal transport through a spin-phonon interacting junction: A nonequilibrium Green's function method study, Phys. Rev. B **96**, 125432 (2017).

[51] J. Ren and J. X. Zhu, Theory of asymmetric and negative differential magnon tunneling under temperature bias: Towards a spin Seebeck diode and transistor, Phys. Rev. B **88**, 094427 (2013).

[52] J. Ren, J. Fransson, and J. X. Zhu, Nanoscale spin Seebeck rectifier: Controlling thermal spin transport across insulating magnetic junctions with localized spin, Phys. Rev. B **89**, 214407 (2014).

[53] N. Mingo, Anharmonic phonon flow through molecular-sized junctions, Phys. Rev. B **74**, 125402 (2006).

[54] J. S. Wang, B. K. Agarwalla, H. Li, and J. Thingna, Nonequilibrium Green's function method for quantum thermal transport, Front. Phys. **9**, 673 (2014).

[55] B. Li, L. Wang, and G. Casati, Thermal Diode: Rectification of Heat Flux, Phys. Rev. Lett. **93**, 184301 (2004).

[56] C. W. Chang, D. Okawa, A. Majumdar, and A. Zettl, Solid-state thermal rectifier, Science **314**, 1121 (2006).

[57] X. K. Chen, J. Liu, Z. X. Xie, Y. Zhang, Y. X. Deng, and K. Q. Chen, A local resonance mechanism for thermal rectification in pristine/branched graphene nanoribbon junctions, Appl. Phys. Lett. **113**, 121906 (2018).

[58] E. Pop, D. Mann, J. Cao, Q. Wang, K. Goodson, and H. Dai, Negative Differential Conductance and Hot Phonons in Suspended Nanotube Molecular Wires, Phys. Rev. Lett. **95**, 155505 (2005).

[59] X. K. Chen, J. Liu, Z. H. Peng, D. Du, and K. Q. Chen, A wave-dominated heat transport mechanism for negative differential thermal resistance in graphene/hexagonal boron nitride heterostructures, Appl. Phys. Lett. **110**, 91907 (2017).

[60] T. Holstein and H. Primakoff, Field dependence of the intrinsic domain magnetization of a ferromagnet, Phys. Rev. **58**, 1098 (1940).

[61] H. Adachi, K.-i. Uchida, E. Saitoh, and S. Maekawa, Theory of the spin Seebeck effect, Rep. Prog. Phys. **76**, 036501 (2013).

[62] S. Streib, N. Vidal-Silva, K. Shen, and G. E. W. Bauer, Magnon-phonon interactions in magnetic insulators, Phys. Rev. B **99**, 184442 (2019).

[63] L. P. Kadanoff and G. Baym, *Quantum Statistical Mechanics: Green's Function Methods in Equilibrium and Nonequilibrium Problems* (Benjamin, Inc., New York, 1962).

[64] L. Keldysh, Diagram technique for nonequilibrium processes, Sov. Phys. JETP **20**, 1018 (1965).

[65] M. P. Lopez Sancho, J. M. Lopez Sancho, and J. Rubio, Highly convergent schemes for the calculation of bulk and surface Green functions, J. Phys. F: Met. Phys. **15**, 851 (1985).

[66] J. S. Wang, J. Wang, and J. T. Lü, Quantum thermal transport in nanostructures, Eur. Phys. J. B **62**, 381 (2008).

[67] F. Guinea, C. Tejedor, F. Flores, and E. Louis, Effective two-dimensional Hamiltonian at surfaces, Phys. Rev. B **28**, 4397 (1983).

[68] N. Mingo and L. Yang, Phonon transport in nanowires coated with an amorphous material: An atomistic Green's function approach, Phys. Rev. B **68**, 245406 (2003).

[69] J. T. Lü and J. S. Wang, Coupled electron and phonon transport in one-dimensional atomic junctions, Phys. Rev. B **76**, 165418 (2007).

[70] T. Frederiksen, M. Paulsson, M. Brandbyge, and A. P. Jauho, Inelastic transport theory from first principles: Methodology and application to nanoscale devices, Phys. Rev. B **75**, 205413 (2007).

[71] F. Giustino, M. L. Cohen, and S. G. Louie, Electron-phonon interaction using Wannier functions, Phys. Rev. B **76**, 165108 (2007).

[72] M. Paulsson, T. Frederiksen, and M. Brandbyge, Modeling inelastic phonon scattering in atomic- and molecular-wire junctions, Phys. Rev. B **72**, 201101(R) (2005).

[73] T. Frederiksen, M. Brandbyge, N. Lorente, and A.-P. Jauho, Inelastic Scattering and Local Heating in Atomic Gold Wires, Phys. Rev. Lett. **93**, 256601 (2004).

[74] Y. Meir and N. S. Wingreen, Landauer Formula for the Current through an Interacting Electron Region, Phys. Rev. Lett. **68**, 2512 (1992).

[75] M. Galperin, A. Nitzan, and M. A. Ratner, Heat conduction in molecular transport junctions, Phys. Rev. B **75**, 155312 (2007).

[76] J. Meair, J. P. Bergfield, C. A. Stafford, and P. Jacquod, Local temperature of out-of-equilibrium quantum electron systems, Phys. Rev. B **90**, 035407 (2014).

[77] J. Li, J. S. Feng, P. S. Wang, E. J. Kan, and H. J. Xiang, Nature of spin-lattice coupling in two-dimensional CrI_3 and $CrGeTe_3$, Sci. China Phys., Mech. Astron. **64**, 1 (2021).

[78] L. Zhang, J. T. Lü, J. S. Wang, and B. Li, Thermal transport across metal-insulator interface via electron-phonon interaction, J. Phys.: Condens. Matter **25**, 445801 (2013).

[79] R. Bosisio, S. Valentini, F. Mazza, G. Benenti, R. Fazio, V. Giovannetti, and F. Taddei, Magnetic thermal switch for heat management at the nanoscale, Phys. Rev. B **91**, 205420 (2015).

[80] K. S. Olsson, K. An, and X. Li, Magnon and phonon thermometry with inelastic light scattering, J. Phys. D. Appl. Phys. **51**, 133001 (2018).

[81] D. T. Larson and E. Kaxiras, Raman spectrum of CrI_3: An *ab initio* study, Phys. Rev. B **98**, 085406 (2018).

[82] T. Ozaki, Variationally optimized atomic orbitals for large-scale electronic structures, Phys. Rev. B **67**, 155108 (2003).

[83] T. Ozaki and H. Kino, Efficient projector expansion for the *ab initio* LCAO method, Phys. Rev. B **72**, 045121 (2005).

[84] J. P. Perdew, K. Burke, and M. Ernzerhof, Generalized Gradient Approximation Made Simple, Phys. Rev. Lett. **77**, 3865 (1996).

[85] A. Togo and I. Tanaka, First principles phonon calculations in materials science, Scr. Mater. **108**, 1 (2015).

[86] M. I. Katsnelson and A. I. Lichtenstein, First-principles calculations of magnetic interactions in correlated systems, Phys. Rev. B **61**, 8906 (2000).

[87] A. Togo and I. Tanaka, SPGLIB: A software library for crystal symmetry search, arXiv:1808.01590 (2018).

[88] Q. Liu, J. J. Li, D. Wu, X. Q. Deng, Z. H. Zhang, Z. Q. Fan, and K. Q. Chen, Gate-controlled reversible rectifying behavior investigated in a two-dimensional MoS_2 diode, Phys. Rev. B **104**, 045412 (2021).

[89] Y. J. Zeng, Y. X. Feng, L. M. Tang, and K. Q. Chen, Effect of out-of-plane strain on the phonon structures and anharmonicity of twisted multilayer graphene, Appl. Phys. Lett. **118**, 183103 (2021).

[90] D. Wu, L. Huang, P.-Z. Jia, X.-H. Cao, Z.-Q. Fan, W.-X. Zhou, and K.-Q. Chen, Tunable spin electronic and thermoelectric properties in twisted triangulene π-dimer junctions, Appl. Phys. Lett. **119**, 063503 (2021).

[91] N. A. Viglin, V. V. Ustinov, S. O. Demokritov, A. O. Shorikov, N. G. Bebenin, V. M. Tsvelikhovskaya, T. N. Pavlov, and E. I. Patrakov, Electric measurement and magnetic control of spin transport in InSb-based lateral spin devices, Phys. Rev. B **96**, 235303 (2017).

[92] H. Haug and A.-P. Jauho, *Quantum Kinetics in Transport and Optics of Semiconductors* (Springer, Berlin, Heidelberg, 2008).

[93] J. Rammer, *Quantum Field Theory of Non-equilibrium States* (Cambridge University Press, Cambridge, 2011).